ANEXOS

I Implementación de un algoritmo utilizando Matlab

El método para la fusión de pilas de proyecciones obtenidas a diferente nivel de energía a partir de una TC ha sido implementado usando Matlab, ya que ofrece una potente y rápida manera de manejar los datos almacenados en matrices. Se han implementado varias funciones para fusionar las proyecciones que son explicadas a continuación.

Abrir.m programado para almacenar las dos pilas de imágenes que van a ser fusionadas en dos matrices, una llamada matrix_H y la otra matrix_L. Dos pilas de imágenes han sido siempre fusionadas (bajo con alto nivel, medio con alto) por ello en matrix_L se almacena la pila de imágenes con menor nivel de energía, y que no tiene porque ser siempre la de baja energía.

Una vez las dos pilas de proyecciones han sido almacenadas, es hora de elegir los cuatro umbrales como muestras las figuras 3.3 y 3.4.

El primer umbral, Xb (del inglés below, bajo) es obtenido a partir del histograma acumulado (histogram.m), correspondiendo con el valor donde acaba el primer pico que corresponde con el metal, el valor es elegido por el usuario a partir de la primera imagen obtenida con un bajo nivel de energía. Se trata de un valor fijo para cada par de imágenes a fusionar, sería mejor si este valor variara con cada par de imágenes, pero debido al gran número de proyecciones, 700, no es posible.

Como se puede ver en la Fig.3.3 y Fig.3.4, hay una correspondencia entre Xb y X1. Una vez Xb es calculado como se ha explicado anteriormente, X1 es el valor de ese mismo pixel en la imagen obtenida con alto nivel de intensidad.

Una vez Xb y X1 han sido calculados se debe hacer lo mismo con Xa y X2.

Xa es usado para separar los píxeles que pertenecen al aire con los que no. Para calcular este umbral, se han seleccionado tres áreas pertenecientes al aire y se ha calculado tanto la media de estos valores como la desviación estándar, a partir de estos valores se obtiene Xa, tres funciones han sido necesarias para este cálculo, white.m, Xabove.m y fused.m.

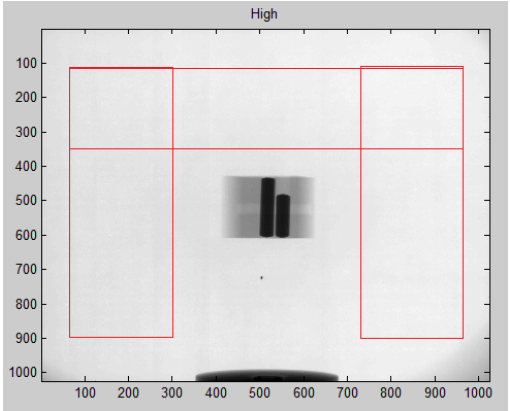

Figura I.1: Tres áreas pertenecientes al aire utilizadas para el cálculo de Xa

Como en el caso anterior, *Xa* es calculado de la imagen obtenida a alto nivel de intensidad y *X2* es el pixel correspondiente en la imagen de bajo nivel de intensidad.

Una vez se tienen los valores para los cuatro umbrales se fusionan las imágenes como se ha visto en las secciones 3.1.1 y 3.1.2., tras la fusión se tiene una nueva matriz llamada $matrix_F$ y con la función writeback.m se guarda esta imagen como un archivo con la extensión .float32 para su posterior reconstrucción.

A continuación se muestran todas las funciones implementadas para la fusión de las pilas de proyecciones.

```
function Boss
%how Matlab has a limited memory that only leave me work with 30 images for
%stack, it is means, 60 images, I have created this loop to process all the
%images together, cleaning the memory each 30 images
for c=1:30:690
    main2(c,c+29)
    clear
end
main2(691,700);
clear;

function main2(down,up)

%matrix_L matrix in where are stored images taken with low intensity
%matrix_H matrix in where are stored images taken with high intensity
%both are 1024x1024 (mxn)
%Xb value of X below thanks to the function histogram
%Xa value of X above thanks to the function white

down  %to know how many time left
up

cap=up-down+1; %to calculate the vector´s capacity

[matrix_H,matrix_L]=abrir(down,up);
matrix_F = zeros(1024,1024,cap);    %new matrix 3D to store the fused images

%size of the matrix
m=1024;
n=1024;


%calculate Xbelow, it means, the lower threshold, from the first image
taken with low intensity

Xb=histogram(matrix_L(:,:,1)); %Xb calculate from the first image

for h=1:cap

    %Now we have to calculated X1
    %is better to work with values higher

    dff=abs(Xb-(matrix_L(:,:,h)));                %I create a new matrix
with the difference between Xb and the image with Low intensity
    [rowL,columnL]=find(dff==min(min(dff)));      %I find where is this
value (in which coordinates)
    rL=rowL(1,1);
```

```
    cL=columnL(1,1);
    X1=matrix_H(rL,cL,h);                          % I store the value of
the pixel with these coordinates as threshold X1


    %Calculate  the upper thershold Xabove from the air which is around the
    %workpiece
    Xa=fused(matrix_H(:,:,h)); %calculated from the function fused.m


    %X2 is calculated from Xa

    dff=(abs(Xa-(matrix_H(:,:,h))));     %I create a new matrix with the
difference between Xa and the image with High intensity
    [rowH,columnH]=find(dff==min(min(dff)));
    rH=rowH(1,1);
    cH=columnH(1,1);
    X2=matrix_L(rH,cH,h);


%we have two options: Upscaling and Downscaling, when one is working the
other one is like a commented


%%
%% UPSCALING
%%
Su=(X2-X1)/(X2-Xb);     %Scaling factor


    for i=1:m
        for j=1:n
          if (matrix_L(i,j,h)<= Xb)           %values smaller than Xb take
the High value
           matrix_F(i,j,h)= matrix_H(i,j,h);
            elseif (matrix_L(i,j,h)>= X2)       %values bigger than Xa take
the Low value
           matrix_F(i,j,h)= matrix_L(i,j,h);
            else
           matrix_F(i,j,h)=Su*(matrix_L(i,j,h)-X2)+ X2;     %scaling values
bewteen Xb and X2
          end
        end

    end


%%
%% DOWNSCALING we check just the high image
%%
%Sd=(X2-X1)/(Xa-X1);
%
%     for i=1:m
%         for j=1:n
%           if (matrix_H(i,j,h)<= X1)           %values smaller than X1
take the High value
%            matrix_F(i,j,h)= matrix_H(i,j,h);
%             elseif (matrix_H(i,j,h)>= Xa)       %values bigger than Xa
take the Low value
```

```
%            matrix_F(i,j,h)= matrix_L(i,j,h);
%             else
%            matrix_F(i,j,h)= Sd*(matrix_H(i,j,h)-X1)+X1;     %scaling
values bewteen Xb and X2
%           end
%          end
%     end
end %for h=1:10


matrix_C=corrected(matrix_F,down,up); %necessary function due to how works
metrotom

%store the new fused images
writeback (matrix_C,down,up);


function [matrix_H,matrix_L]= abrir(down,up)
%open files taken with high intensity and store it in a 3D matrix called
%matrix_H
%open files taken with low intensity and store it in a 3D matrix called
%matrix_L

cap=up-down+1; %cap is the capacity or dimension to the matrix_H and
matrix_L

matrix_H = zeros(1024,1024,cap);

for j=down:up
        filename=strcat('H(',num2str(j),').float32');

        fileID = fopen(filename);
        for i = 1:1024
            h=j-(down-1);
            matrix_H(i,:,h)=fread(fileID, 1024, 'float32');
        end
        status = fclose(fileID);

end

 matrix_L = zeros(1024,1024,cap);

 for j=down:up
        filename=strcat('M(',num2str(j),').float32');

        fileID = fopen(filename);
        for i = 1:1024
            h=j-(down-1);
            matrix_L(i,:,h)=fread(fileID, 1024, 'float32');
        end
        status = fclose(fileID);

end

function [Xb]= histogram(matrix)
%Where Xb is directly Xbelow, this means, the below threshold
%Xb is only once calculated, with the first file taken with low intensity
```

```
imhist(matrix)
axis([0  1  0  5000])

%to choose the threshold Xbelow
disp('Choose the threshold and push enter: ');
[x,y] = ginput;

disp(['You have chosen a threshold of ',num2str(x)]);
Xb=x;
close();

function Xa=fused (A)
%to calculate the above threshold superior as average between each Xabove
%
%A is the area selected

B=white(A,100,100,300,700);
X1=Xabove(B);
B=white(A,200,100,800,200);
X2=Xabove(B);
B=white(A,700,100,900,700);
X3=Xabove(B);
Xa=(X1+X2+X3)/3;

function B=white(A,a,b,c,d)
%A full image
%a,b coordinate of the upper left corner
%c,d coordinate of the lower right corner
%B area of an image

B=A(a:c,b:d);

function Xa = Xabove (A)
%Xa is the difference between the mean and the standar desviation of the
values of a matrix

mu = mean(mean(A));
s=std(std(A));
Xa=mu-s;

function matrix_C=corrected(matrix_F,down,up)
%function necessary to correct all the fused images

matrix_W = zeros(1024,1024);
matrix_S = zeros(1024,1024);

fileID = fopen('weissReal.float32');
        for i = 1:1024
            matrix_W(i,:)=fread(fileID, 1024, 'float32');
        end
        status = fclose(fileID);

fileID = fopen('schwarzReal.float32');
        for i = 1:1024
            matrix_S(i,:)=fread(fileID, 1024, 'float32');
        end
        status = fclose(fileID);
```

```
cap=up-down+1; %cap is the capacity or dimension of the matrix_H and
matrix_L


 m=1024;
 n=1024;

 matrix_D = zeros(1024,1024);
 matrix_C = zeros(1024,1024,cap);
%difference between weiß - Schwarz
for i=1:m
        for j=1:n
             matrix_D(i,j)=matrix_W(i,j)-matrix_S(i,j);
        end
end

%(difference x Fused) + Schwarz
for h=1:cap
    for i=1:m
        for j=1:n
           matrix_C(i,j,h)= (matrix_D(i,j)*matrix_F(i,j,h))+matrix_S(i,j);
        end
    end
end

function writeback (matrix_F,down,up)
%program to create the new fused files from matrix_F

for j=down:up
     filename=strcat('Uncorrected',num2str(j+1),'.float32');
     fid = fopen(filename,'wb');

     for i = 1:1024
        h=j-(down-1);
        fwrite(fid,matrix_F(i,:,h),'float32');
     end

     status = fclose(fid);

end
```

Hasta aquí se han mostrado las funciones necesarias para fusionar las pilas de proyecciones, las siguientes funciones son las utilizadas para el análisis de los cortes realizados al volumen en 3D.

```
function  abrir
%open the corresponding stacks of slices and evaluate a profile

cap=315;    width=420;  height=420;

 matrix = zeros(width,height,cap);

for h=1:cap
        filename=strcat('DownMH',num2str(h-1),'.raw');
        fileID = fopen(filename);
        for i = 1:width
            matrix(i,:,h)=fread(fileID, width, 'uint16');
```

```
        end
        status = fclose(fileID);
end


 for h=1:cap

  imagesc(matrix(:,:,h)); title('Downscaling');   colormap(gray);
  improfile;

    pause;
end

close all;
clear;

function  valuePixel
%with this function, after of choosing the upper left corner and the lower
right corner in an image, it calculate the mean and the standard deviation
from the chosen area

cap=315;    width=420;  height=420;

filename=strcat('DownMH130.raw');       %First to must choose which image
you are going to work
        fileID = fopen(filename);
        for i = 1:width
            matrix(i,:)=fread(fileID, width, 'uint16');
        end
        status = fclose(fileID);

  imagesc(matrix); title('Downscaling');   colormap(gray);

    disp('Choose the upper left corner ');
    [xo,yo] = ginput;
    xo=xo-mod(xo,1)
    yo=yo-mod(yo,1)

    disp('Choose the lower right corner ');
    [x1,y1] = ginput;
    x1=x1-mod(x1,1)
    y1=y1-mod(y1,1)

    %A full image
    %a,b coordinate of the upper left corner
    %c,d coordinate of the lower right corner
    %B area of an image
    B=matrix(yo:y1,xo:x1)
    pause;

    %the mean and the standard deviation of the values of a matrix
    mu = mean(mean(B))
    s=std(std(B))
    pause;

close all;
clear;
```

II Memoria en inglés

Diplomarbeit

Cand.-Ing.: Cristian Piedrafita

Matr.-Nr.: 299597

Theme: Enhancing the inspection of multi material work pieces with industrial computed tomography

Supervising Assistant: Dipl.-Ing. Sebastian Pollmanns

Aachen, den 17.06.2010

Contents

II.1 Introduction

The development of this Master Thesis has taken place at the Laboratory for Machine Tools and Production Engineering WZL of the RWTH Aachen University, Germany, in the department of Production Metrology Quality Management. The supervision of the project has been carried out by the team leader Dipl.-Ing. Sebastian Pollmanns.

The RWTH Aachen is the largest technical university in Germany and one of the most renowned in Europe. There are currently around 30,000 students, the majority of them in mechanical engineering. With almost 11,000 employees, the RWTH is the largest employer in the region. The machine tool lab (WZL) at the RWTH Aachen stands for innovation in production technology. The entire depth of the subject is represented by six professorships with a total of 600 employees. Against this background, the experts of the chair for Production Measuring Technology and Quality Management from Prof. Dr. Robert Schmitt are working on practical solutions for different industries. For this, integration concepts are being developed and customized for implementation in companies, and metrology procedures for practical use are being developed, qualified and optimized. Manufacturing companies thus receive support while enhancing their competitiveness.

The research area of Production Metrology and Quality Management operates within the scopes of development and Optimization of Measurement Technologies and Machines, Production Integrated Metrology, Quality Management Systems and Methods as well as Knowledge-, Innovation- and Optimization Management.

A METROTOM 1500 computed tomography from Carl Zeiss [ZEIM10] is used at the WZL for CT measurements. Measurements with the computed tomography – with X-rays – provide clear benefits: work pieces can be easily and completely examined. They are then available as virtual 3D models. In addition to visualization and segmenting possibilities, a volume model can also be used to measure the required geometric features.

Figure II.1: Metrotom 1500

II.1.1 Initial situation and current limitations in the application of computed tomography

X-ray computed tomography (CT) has experienced tremendous growth in recent years, in terms of industrial and medical applications. Many advantages have been achieved in major CT components, such as tube, detector, slip ring, data acquisition systems, and algorithms [HSIE03, P. 1-2].

The application of industrial computed tomography (CT) for the inspection and geometrical characterization of work pieces within the scope of quality assurance is growing rapidly. The main potential of this technology is related to the capability of acquiring volumetric data with high resolution in extern as well as in intern regions of the part that can be further analyzed for e.g. in the field of material testing to non-destructive testing.

However some limitations still exist to the applications of CT. Up to now the usage of industrial CT is limited to work pieces made from one material or combinations with nearly densities. At first it is not possible to measure objects of high aspects ratios (ratio width to thickness) as the changing material thickness influence the remaining intensity after the radiation passed through the work piece. Secondly parts consisting of different absorbing materials cannot be measured as only the high absorbing components are acquired with good signal-to-noise ratio, i.e. with high accuracy and low measurement uncertainty.

A remaining intensity must be secured after the radiation passed the thickest part of the sample, varying the radiation and acquisition parameters (e.g. voltage, current, integration time). Without remaining intensity the reconstruction will not lead to proper and usable results. As high radiation energies are necessary to assure remaining intensities greater than zero in the radiographs, low absorbing components are outshined and not visible after reconstruction [KRÄM10]. Also the inspection of multi material work pieces e.g. made of plastic and metal currently suffer from imaging artifacts that occur during the reconstruction process and that reduce the quality of the volumetric model significantly.

II.1.2 Goals

The way to develop this Master Thesis is based on the fusion of two projection image stacks (about 700 files) taken with different energies to obtain a good remaining intensity in all different kind of materials. With this method, the target is to obtain a correspondence between every pixel taken with low and high energy, so as to obtain a new image in which the different materials are clearly visualized.

This method requires avoiding movement of the work piece while the two image stacks are taken. To facilitate the fusion both stacks have to consist of the same amount of projection taken with the same degree variation.

The problem is the acquisition of a work-piece consisting of several materials, because there are different capacities of absorbing, so the parameters may be either optimized for one material or another one. For example metal is highly absorbing, if the parameters are optimized for this material, the plastic component will be overexposed and outshined in the projection image. The situation may even be worse if the acquisition process is optimized for

the plastic components, because the lower energy of the radiation may not be sufficient to pass through the metal parts. Therefore the remaining intensity behind the metal parts is equal to zero, which makes the back-projection of these parts impossible. In these cases it is necessary to take a special care with artifacts, which appear especially with low intensity, the reason of these errors or artifacts will be explained later.

For all these reasons, the main goal of this Master Thesis is the development of an algorithm that allows an appropriate fusion of the different stacks of images

II.1.3 Structure of the work

After this first chapter, where the current limitations in computed tomography and objectives for the project were introduced, the next chapters are divided as in the following part:

Chapter 2, State of the art, the basic principles of computed tomography and how it operates are explained. There is also a short summary of the history of CT, where the development of CT can be seen. Another important section inside this chapter is the one which refers to the artifacts in images, where the different artifacts and their appearance are explained. It is important to know about them because the objective is to reduce them. In the end of this chapter, there is a brief description about previous studies that have also used the image fusion and the relationship with this work.

Chapter 3, Development of a fusion algorithm for projection images, explains the idea which is used for the fusion of images, both upscaling and downscaling, and necessity of the scaling. There is also a description of the program implemented in Matlab which makes it possible.

In Chapter 4, Performing of an experimental study is shown. The experimental plan proves the different experiments. It is also explained the evaluation criteria followed and finally present the results.

To end Chapter 5 contains the evaluation of the results where they are commented and Chapter 6 conclusions and outlook, which it contains possible improvements for future researches.

II.2 State of the art

X-ray radiation is an electromagnetic waveform, like microwaves, infrared, visible light, ultraviolet, and radio waves. The wavelength of the X-ray ranges from a few pico-meters to a few nanometers. The energy of each X-ray photon, E, is proportional to its frequency, v. and is described by the following expression:

$$E = hv = \frac{hc}{\lambda} \qquad \textbf{Eq2.1}$$

where h is Planck's constant and equals (6.63 x 1064 J s), c is the speed of light ($3 \cdot 10^8$m/s), and λ is the wavelength of the X-ray. Therefore, X-ray photons with longer wavelengths have lower energies than the photons of shorter wavelengths. For convenience, the X-ray energy is usually expressed in units of eV (1 eV = 1.602 x 10*9 J). This is the amount of kinetic energy with which an electron is accelerated across an electrical potential of 1 V (the actual

energy equals the product of the electron charge times the voltage). Because X-ray photons are produced by striking a target material with high-speed electrons (the kinetic energy is transformed into electromagnetic radiation), the maximum possible X-ray photon energy equals the entire kinetic energy of the electron. The next equation can then be converted into units of eV:

$$E = \frac{1.24\ x\ 10^3 eV \cdot nm}{\lambda} \qquad \textbf{Eq2.2}$$

X-rays with wavelengths in the range of 10 nm (124 eV) to 0.1 nm (12.4k eV) are often called soft X-rays, because of their lack of ability to penetrate thicker layers of materials. These x-rays have less value in radiology. The wavelength of diagnostic X-rays varies roughly from 0.1 nm to 0.01 nm, corresponding to an energy range of 12.4 keV to 124 keV. Although x-rays with much shorter wave-lengths are highly penetrating, they provide little low-contrast information and, therefore, are of little interests to diagnostic imaging. It is worth pointing out that X-rays are at the high-energy (short wavelength) end of the electromagnetic spectrum [HSIE03, P. 28]. To illustrate, Fig. 2.1 depicts the electromagnetic spectrum, with different types of electromagnetic waves labeled.

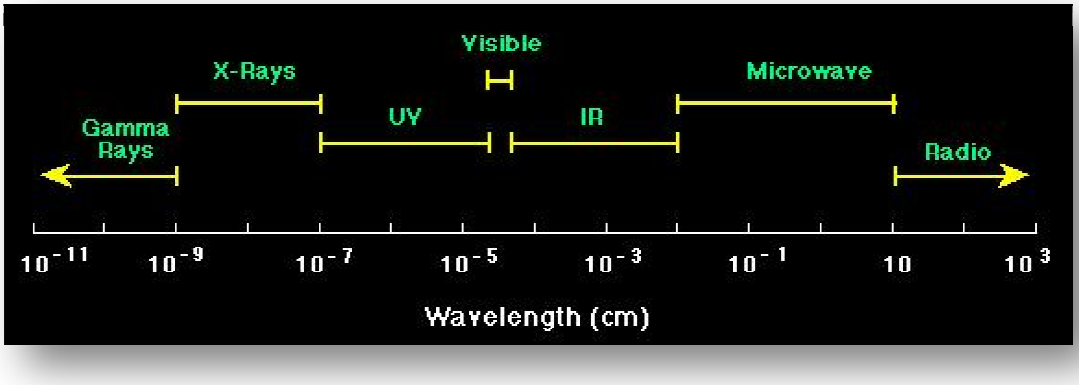

Figure II.2: Illustration of the electromagnetic spectrum [CSEP10]

The typical energy range of the X-ray photons generated for medical CT is between roughly 20 keV and 140 keV. On the other hand the industrial CT with which the stacks of images have been taken has an energy range between 80 keV and 225 keV [HEIN08]. In this energy range, there are three fundamental ways in which X-rays interact with matter: the photoelectric effect, the Compton Effect, and coherent scattering [HSIE03, P. 31-34], the net effect of these interactions is that some of the photons are absorbed or scattered. In other words, X-ray photons are attenuated when they pass through a material. The attenuation can be expressed by an exponential relationship for a monochromatic (monoenergetic) incident X-ray beam and a material of a uniform density and atomic number.

$$I = I_0 e^{-(\tau+\sigma+\sigma_r)L} \qquad \textbf{Eq.2.3}$$

Where I and Io are the incident and transmitted X-ray intensities, and L is the thickness of the material (cm). $\tau, \sigma \; and \; \sigma_r$ are the attenuation coefficients of the photoelectric, Compton, and coherent scattering interactions of the material, respectively. The above equation is often expressed as:

$$I = I_0 e^{-\mu L} \qquad \textbf{Eq.2.4}$$

where μ is the linear attenuation coefficient of the material. This is often called the Lambert-Beers law.

II.2.1 Computed Tomography

The first CT has been developed for medical applications by Sir Godfrey N. Hounsfield at EMI Central Research Laboratories in 1971 after Wilhelm Conrad Röntgen had discovered the X-rays already in 1895, Johann Radon had demonstrated the mathematical roots for the today used back projections algorithms in 1917 and Cormack had developed the theoretical fundamentals at the beginning of the 1960s. This revolutionary technology for which Hounsfield and Cormack received the Nobel Prize in Physiology or Medicine in 1979, allowed new insights into the human body and was such rapidly adopted in the fields of medicine diagnostics. Many developments from the increased distinction of smaller density differences to the faster speed of measurements made the technology suitable for non-destructive testing purposes. At first it was used for security-relevant inspections, e.g. of helicopter o turbine blades, and later on the use was expanded to the inspection of casted aluminum parts. In this area even the first dimensional inspections were carried out to analyze wall thicknesses in addition to the detection of flaws and other inhomogeneities. Around the year 2000 improved equipment, especially more sensitive detectors, tubes with smaller focal sports and improved reconstruction algorithms made the use of CT dimensional metrology possible [WECK09].

II.2.2 Working principle of CT

Since the development of X-ray Computed Tomography (CT) and its rapid acceptance in medical diagnostics, it became not only a powerful tool for non-destructive testing but was also adopted in manufacturing metrology in the last decade. CT offers new possibilities for coordinate measurements as it is possible to acquire a volumetric model of the entire work piece with a single measurement at which analyses known from coordinate metrology such as estimation of geometric features or nominal/actual value comparisons can be performed. But with data sets generated by tomography measurements it is also possible to analyze the entire volume of the work piece, so detection and analysis of conventionally not accessible features like defects (flaws, blow holes, bubbles) or wall thickness analyses with uncertainties in the micrometer range are possible.

The measurement principle of Computed Tomography as shown in Fig.2.2, relies on the attenuation of radiation by the measurement object which is dependent on the material (atomic number, density) and the path length of the X-rays.

Compared to medical CT, industrial CT uses a different principle, the principle of common industrial CT, also referred to as cone beam CT. The tube emits high energy X-ray radiation (E~ 80-225 keV) which is partly absorbed by the measurement object and the remaining intensity is detected by silicon flat panel detectors which mostly even offer the possibility of examining the work piece in real-time by 2D weakening images known from radiography [WECH09].

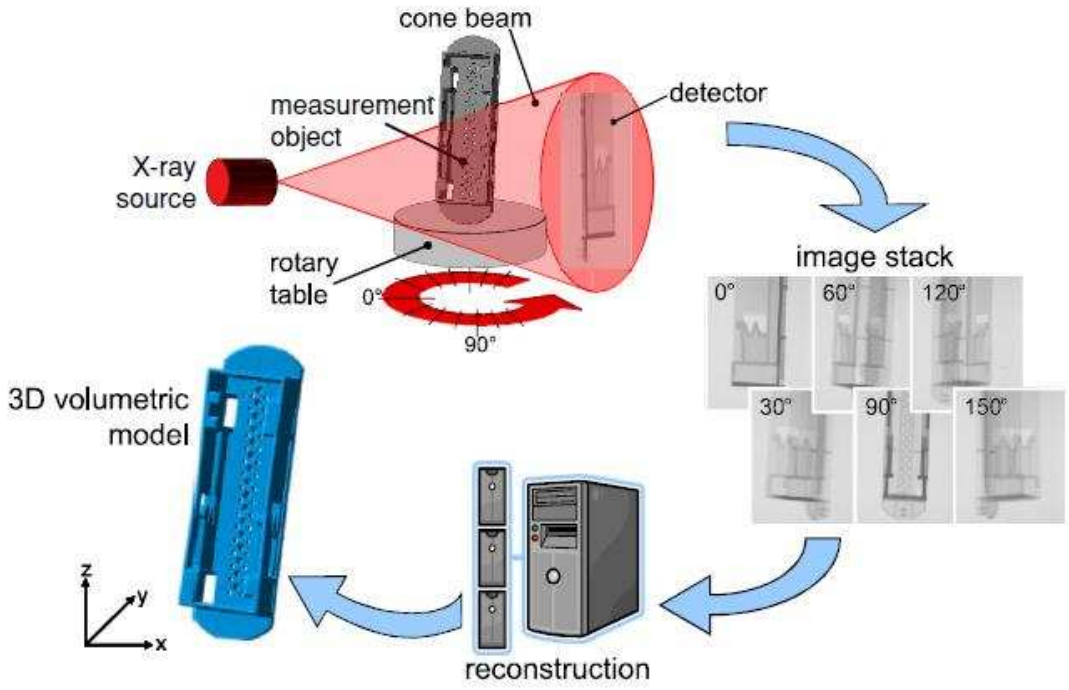

Figure II.3: Basic principle of industrial computed tomography [WECH09]

Unlike in radiography not only a single weakening image is evaluated, the work piece is rotated by 360º and in a user-definable amount of angle positions images are acquired. This is important for the quality of the measurement results but it is also the greatest factor which influences the needed measurement time. Additionally several images at a single angle position can be combined to reduce the noise in a single projection image but it also multiplies the measurement time [KAST04].

One of the main characteristic of X-rays is their polychromatic spectrum. The source emits radiation from different wave lengths and energies. This leads to one of the main influences in computed tomography, so called beam hardening.

As the radiation passes through the measurement object the absorption of low energy which changes the spectrum towards higher (“harder”) energy, the radiation seems to consist of more energetic, harder radiation. For dimensional analyses this non-linearity makes it more difficult to calculate the length of the way of the radiation through the measurement object during the reconstruction process which leads to systematic errors, e.g. in the estimation of diameters [WECH09].

Together these projections form an image stack which can be reconstructed by mathematical algorithms based on Radon´s work already published in 1917 and implemented by Feldkamp in 1984 [FELD84]. To increase the image quality and therefore the quality of the resulting

volumetric model, the projections are filtered before the back projection, that why this reconstruction method is called “filtered back projection” (FBP), which is the most common, used image reconstruction method in CT. FBP assumes that every X-ray beam used for image reconstruction is monoenergetic. Under this assumption, there is a linear relation between measured attenuation data and the thickness of a given material. Although in reality the X-ray beams are polyenergetic. Passing through an object lower energetic X-ray beams are attenuated more by a given tissue material than higher energetic X-ray beams. Therefore, the total attenuation is no longer a linear function of the objects thickness. To reduce this problem CT scanners are typically equipped with correction software that is optimized for body tissue including bone (medical CT), but not for high attenuation objects like metal. In addition, many other sources of streak artifacts exist like photon starvation, scattering edge gradient effect and motion [MAHN03].

The data set resulting from reconstruction consists of volumetric elements (voxels) where each of them represents a specific gray value which is proportional to the acquired radiation intensity. So the voxels are the 3D equivalent of the pixels known from 2D images [WECH09].

II.2.3 Imaging Artifacts within CT-Measurements

The definition of an image artifact is not as clearly defined as one might expect. Theoretically, an image artifact can be defined as any discrepancy between the reconstructed values in the image and the true attenuation coefficients of the object. Compared with the conventional radiography, CT systems are inherently more prone to artifacts, due to a CT image is generated with a larger number of projections, (in our case about 700). In a typical CT system, each projection contains roughly 1000 separate measurements. (in the case of a multislice CT scanner, the number of measurements in a single projection can easily be quadrupled). As a result nearly of 10^6independent readings or measurements are used to form an image. Because of the nature of the back projections process that maps a point in a projection to a straight line in an image, an error in the projection reading is no longer localized, like in conventional radiography. Since inaccuracies of the measurements are usually manifested as errors in the reconstructed images, the probability of producing an image artifact is much higher for CT [HSIE03; P.167].

Generally speaking, CT image artifacts can be classified into four major categories: streaking, shading, rings and bands, and miscellaneous [HSIE03; P.167-168].

It is possible to group the origins of these artifacts into four categories: (a)physics-based artifacts, which result from the physical processes involved in the acquisition of CT data; (b)work piece-based artifacts, which are caused by such factors as work piece movement or the presence of metallic materials in or on the work piece; (c) scanner-based artifacts, which result from imperfections in scanner function; and (d) helical an multisection artifacts, which are produced by the image reconstruction process.

II.2.3.1 Physics-based Artifacts

The CT reconstruction algorithm is based on the assumption that a particular volume element attenuates all X-rays in the same way independent of the projection angle or propagation path length. Therefore, the linear attenuation coefficient μ changes nonlinearly along the propagation path. Hence, the reconstructed image of the specimen seems to have changing densities depending on the location in the volume. Most materials absorb low-energy X-rays better than high-energy X-ray photons, mainly because of photoelectric absorption. A typical material has a high attenuation coefficient for low-energy photons and a low attenuation coefficient for high-energy photons. For example, when X-ray photons with different energies are directed at a layer of soft tissue, photons with lower energies will be absorbed more than the higher-energy photons. Photons with energies below 10 keV are almost totally absorbed; consequently, a heterogeneous X-ray beam becomes proportionately richer in high-energy photons (more penetrating, or “harder”). [KRUM08] [HSIE03; P.221-223] [BARR04]

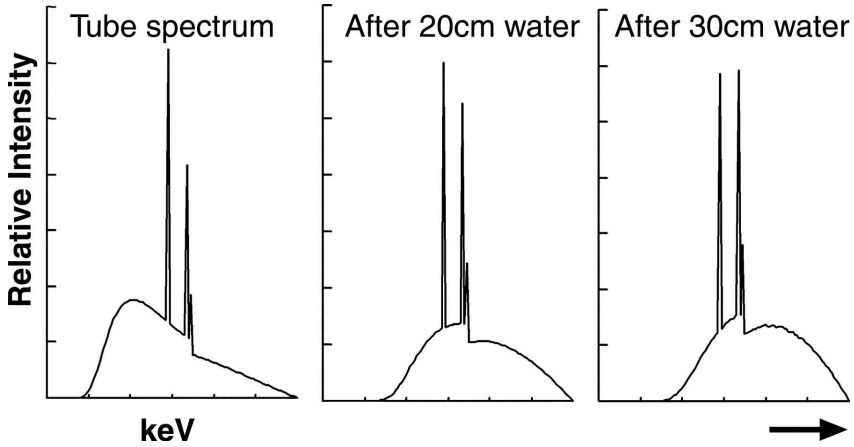

Figure II.4: Changing energy spectrum of an X-ray beam as it passes through water. The mean energy increases with depth. (The attenuated spectra have been rescaled to be equivalent in size to the unattenuated spectra) [BARR04]

For this reason this effect is called beam hardening and two types of artifacts can result from this effect: so-called cupping artifacts and the appearance of dark bands or streaks between dense objects in the image.

II.2.3.1.1 Cupping Artifacts

X-rays passing through the middle portion of a uniform cylindrical phantom are hardened more than those passing though the edges because they are passing though more material. As the beam becomes harder, the rate at which it is attenuated decreases, so the beam is more intense when it reaches the detectors than would be expected if it had not been hardened. Therefore, the resultant attenuation profile differs from the ideal profile that would be obtained without beam hardening (Figure 2.4) [BARR04].

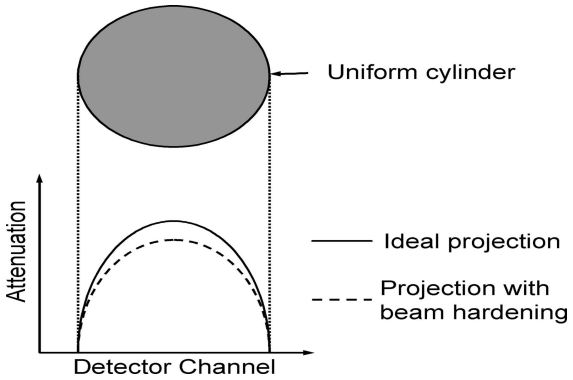

Figure II.5: Attenuation profiles obtained with and without beam hardening for an X-ray beam passing through a uniform cylindrical phantom [BARR04]

II.2.3.1.2 Streaks and Dark Bands

Streaking artifacts often appear as intense straight lines (not necessary parallel) across the image. They can be either bright or dark. In many cases, the bright and dark streaks appear in pairs because of the nature of the reconstruction filter. When they appear in large quantities and large magnitudes, these artifacts can degrade the image quality to such an extent that images become either unreadable or unreliable. They occur because the portion of the beam that passes through one of the objects at certain tube positions is hardened less than when it passes through both objects at other tube positions. A streak is usually caused by inconsistency present in isolated measurements, the inconsistency could be the result of an inherent problem associated with the data collection process, mechanical malfunction, abrupt changes between views or too many noise, because excessive photon noise can cause severe streak artifacts. [KRUM08] [HSIE98].

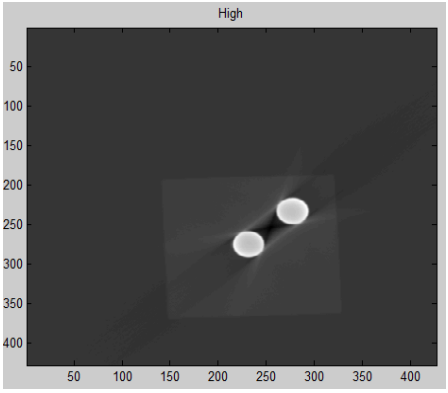

Figure II.6: Example of Streaks and Dark Bands in the model used

II.2.3.2 Workpiece-based Artifacts

The presence of metal objects in the scan field can lead to severe streaking artifacts. They occur because the density of the metal is beyond the normal range that can be handled by the computer, resulting in incomplete attenuation profiles. Additional artifacts due to beam hardening, partial volume, and aliasing are likely to compound the problem when scanning very dense objects [BARR04].

Different approaches towards metal artifact reduction were describes, including physical prefiltering, water correction, and dual energy scanning. Many different post-processing algorithms for metal artifact reduction were published as well. [DEMA00] [MORI81] [TUY93].

II.2.3.3 Scanner-based Artifacts

II.2.3.3.1 Ring artifacts

If one of the detectors is out of calibration on a third-generation (rotating X-ray tube and detector assembly) scanner, the detector will give a consistently erroneous reading at each angular position, resulting in a circular artifact (Fig 2.6). A scanner with solid-state detectors, where all the detectors are separate entities, is in principle more susceptible to ring artifacts than a scanner with gas detectors, in which the detector array consists of a single xenon-Filled chamber subdivided by electrodes.

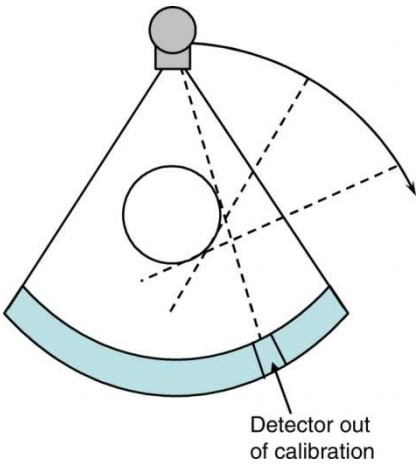

Figure II.7: Formation of a ring artifact when a detector is out of calibration [BARR04]

A ring artefact manifests itself as circular streaks around the centre of rotation of the object under examination. It is caused by differences in detector response during the data acquisition process, and is exacerbated by the beam-hardening non-linearities. These artifacts are typically found in rotate-only type scan geometries [ISO 15708-2:2002(E)].

They can impair the diagnostic quality of an image, and this is particularly likely when central detectors are affected, creating a dark smudge at the centre of the image.

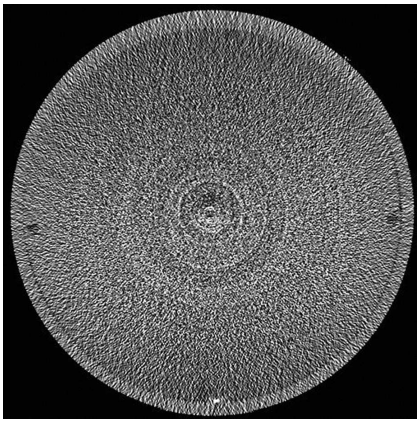

Figure II.8: CT image of a water-filled phantom shows ring artifacts [BARR04]

The presence of circular artifacts in an image is an indication that the detector gain needs recalibration or may need repair services. Selecting the correct scan field of view may reduce the artifact by using calibration data.

All modern scanners use solid-state detectors, but their potential for ring artifacts is reduced by software that characterizes and corrects detector variations.

II.2.3.4 Helical and Multisection CT Artifacts

In general, the same artifacts are seen in helical scanning as in sequential scanning. However, there are additional artifacts that can occur in helical scanning due to the helical interpolation and reconstruction process. The artifacts occur when anatomic structures change rapidly in the z direction (e.g. at the top of the skull) and are worse for higher pitches.

II.2.4 Image fusion

Image fusion is defined as the process of combining information in two or more images of a scene to enhance viewing or understanding of the scene. Image fusion, as opposed to strict data fusion, requires data representing every point on a surface or in space so be fused, rather than selected points of interest [GOSH05].

Image fusion is a growing topic for medical, military, and industrial applications. There are numerous medical examples presented of image fusion for registering and combining magnetic resonance (MR), positron emission tomography (PET), and computed tomography (CT) into composites to aid surgery [DERE94].

In the field of industrial application there are many different uses of the image fusion that includes non-destructive (NDE) evaluation techniques to inspect [BLUM05]. In each of these examples, there are numerous opportunities for image fusion success in bringing together images from different sensors to help indecision making and diagnostics.

Some benefits of image fusion include:

- Image overlay for displays
- Image sharpening for operator clarity
- Image enhancement through noise reduction
- Image mosaicking for enhanced spatial coverage
- Image registration for reference to world coordinates
- Enhanced clarity through feature amplification
- Segmentation through regional selections
- 3D estimation for scene calibration
- Image identification for tracking

As it can be seen there are many applications in the field of industrial applications in which the image fusion is used.

The first idea to develop this Master Thesis has been obtained from the technique called HDRi (High Dynamic Range Imaging). In image processing, computer graphics, and photography, HDRi is a set of techniques that allow a greater dynamic range of luminances

between the lightest and darkest of an image than standard digital imaging techniques or photographic methods. This wider dynamic range allow HDR images to more accurately represent the wide range of intensity levels found in real scenes, ranging from direct sunlight to faint starlight [MYSZ05].

It is not exactly the same way to proceed, but the main idea is the same. It is to take a several photos obtained with different level of intensity in order to obtain a fusion image where the entire characteristic have a better definition.

II.3 Development of a fusion algorithm for projection images

As mentioned previously, working at high intensity can reduce the number of artifacts present in metal. For this reason, the fused images will have the same pixels in metal than those taken at high intensity.

In the same way, due to low air density, the air is better defined at low intensity. Therefore the fused images will have the same pixels in the air than the image taken with low level of intensity.

II.3.1 Theorical Basis

All the process to fuse the image comes from Lambert-Beers law, Eq2.1, function which has a logarithmic form. In the next figure is shown a model how our vision of the penetration of a homogeneous material is when the stacks of images are taken with low, medium and high level of intensity.

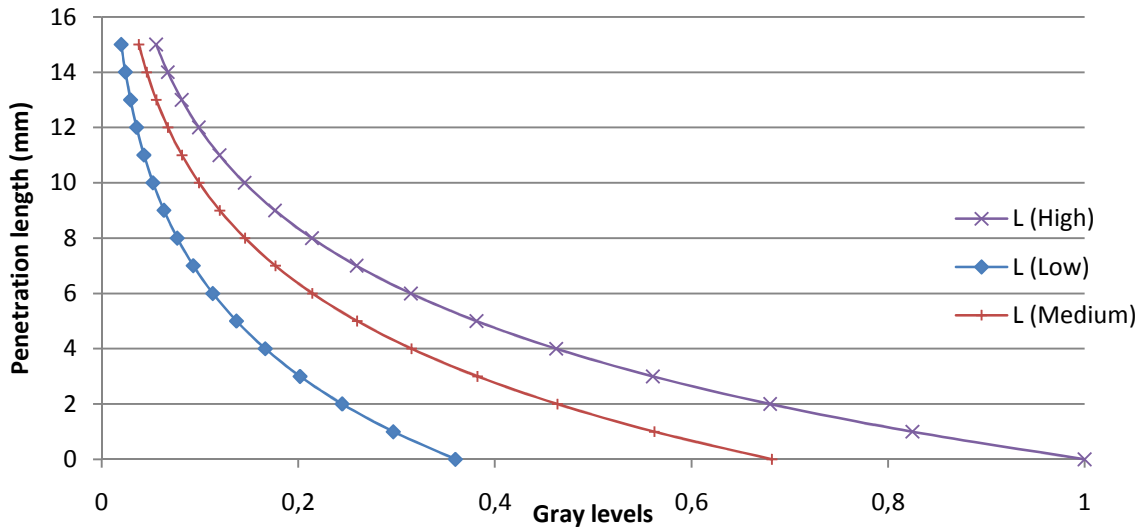

Figure II.1: Logarithmic function for the penetration of a homogeneous material

In the x-axis are represented the gray levels, and in the y-axis the penetration length.

The x-axis is between 0 and 1 because the projections calculated with Metrotom give us the values of the pixels in floating point, for this reason the levels of gray are between 0 and 1, where 0 is black and 1 is white. The y-axis shows the length and it is between 0 and 15.5 because it is half diagonal of the cube.

The idea to fuse the images has been taken from this plot, because one of the most important goals of this Master Thesis is to find a way to fuse the stack of images. A new fused image from pixels from both image stacks has been made.

Considering that the two image stacks have been acquired using different energies the corresponding pixels of two projections do not have matching gray values. So a scaling of one image stack to fit the other has been done using a scaling factor S. There are different possibilities to apply this factor to the data:

- Upscaling

- Downscaling

Both upscaling and downscaling need a prior data collection of the thresholds Xb, X1, X2 and Xa, Fig.3.3 and 3.4 show the four thresholds, as a brief description it can be said that Xb is the limit of the metal with the plastic; Xa is used to separated pixels that belong to the air with the rest of pixels that do not belong to the air; X1 has a correspondence with Xb and X2 with Xb. They will be explained with more detail in the section 3.2 Implementation of the algorithm by using Matlab.

On the one hand, the method of upscaling has been applied for the pixels with values between Xb and X2 in the image taken with low intensity (see Fig.3.2 to clarification), and as its name implies, these values have been multiplied by a factor Su to increase its value of gray level.

On the other hand, the downscaling has been applied for the pixels with values between X1 and Xa (see Fig.3.3), in this case the pixels have seen its value decreased.

II.3.1.1 Upscaling

The thresholds Xb and Xa and the corresponding X1 and X2 have been calculated how is going to be explained in the next section 3.2 Implementation of the algorithm by using Matlab. When the method of upscaling is applied, the pixels between Xb and X2 in the low curve have to be upscaled to the high curve as it is shown in Fig.3.2, to avoid mismatch of gray levels.

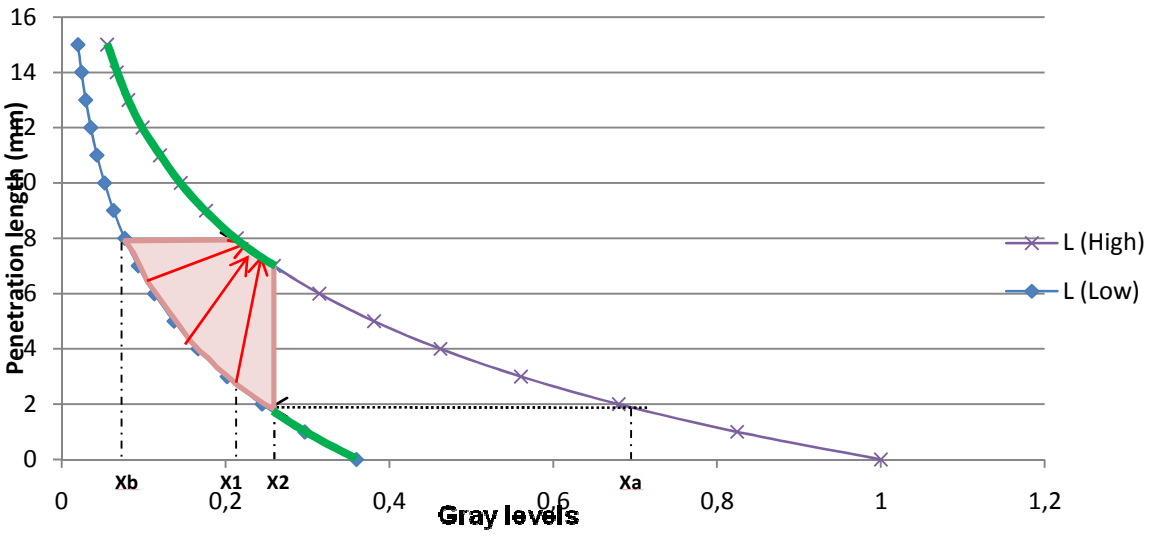

Figure II.2: Upscaling

In order to do this numerically a factor of scaling is needed, as we have to upscale all the pixels between Xb and X2 in the low curve in points between X1 and X2 in the high curve, the factor of upscaling will be the following form:

$$Su = \frac{(X2-X1)}{(X2-Xb)} \qquad \textbf{Eq.3.1}$$

Once this value Su has been calculated we have operate with the same equation to calculate the new values:

$$Su = \frac{(X2 - matrix_{F(i,j)})}{(X2 - matrix_{L(i,j)})} \quad \textbf{Eq.3.2}$$

After isolating the variable $atrix_{F(i,j)}$:

$$matrix_{F(i,j)} = Su * \left(matrix_{L(i,j)} - X2\right) + X2 \quad \textbf{Eq.3.3}$$

The rest of values between X1 and X2 in the high image have been obtained due to this equation and the factor Su.

The new fused pixel in the position (i,j) corresponds with $matrix_{F(i,j)}$ and $matrix_{L(i,j)}$ is the pixel in the low Image in the position (i,j).

After using upscaling, the fused image (or stack of fused images) is consisted with pixels that belonging with the green line in Fig.3.2, where can be observed that metal, plastic and air are represented without gray levels jumps between them, which would not have been possible without the scaling.

II.3.1.2 Downscaling

Another option to calculate the new values of the pixels is downscaling. It is nearly similar to the previous case but with a little difference:

Now the pixels are between X1 and Xa in the image taken with high energy, which must be recalculated.

The next image shows how must be calculated this factor Sd:

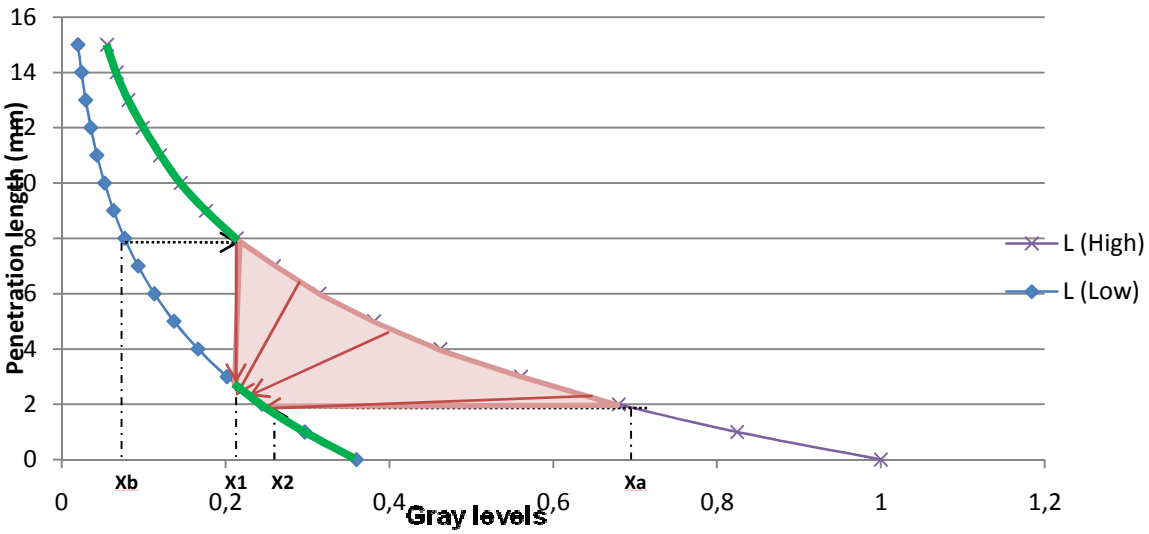

Figure II.3: Downscaling

Now the new values for all the pixels between X1 and Xa in the high image have been recalculated. The factor is calculated similar to the upscaling method, but now changing the thresholds.

$$Sd = \frac{(X2 - X1)}{(Xa - X1)} \quad \textbf{Eq.3.4}$$

After replace the variables and isolate $matrix_{F(i,j)}$:

$$Sd = \frac{(matrix_{F(i,j)} - X1)}{(matrix_{H(i,j)} - X1)} \quad \textbf{Eq.3.5}$$

$$matrix_{F(i,j)} = Sd * \left(matrix_{H(i,j)} - X1\right) + X1 \quad \textbf{Eq.3.6}$$

In this case $matrix_{H(i,j)}$ is the pixel in the position (i,j) in the image taken with high intensity.

The fused image is made with pixels that belonging with the green line in Fig.3.3. As in upscaling, there is continuity in gray levels thanks to scaling.

II.3.2 Implementation of the algorithm by using Matlab

The method for fusion of multi-energy CT image stacks described above has been implemented using MATLAB as it offers powerful and fast ways to handle matrix image data. Several functions have been implemented in order to fuse the images, in the next pages these functions are going to be explained.

Abrir.m has been programmed to load two stacks of images which are going to be fused, in two matrixes, one called matrix_H and the other one matrix_L. Two stacks of images have been always fused (medium with high, low with high); so matrix_L store the stack of images taken with less level of intensity, not necessarily the stack taken with low intensity also can be the medium when it is fused with the high.

Once the two stacks of images have been stored, it is time to choose the four thresholds as is shown in the Fig.3.2 and Fig.3.3.

The first one Xb (below) is obtained from the accumulated histogram (histogram.m), corresponding with a value where the first peak ends; this value is chosen by the user from the first image obtained with low energy. It will be better if this value would be chosen every time for every image, but as there are 700 images is not usable, so in each fusing a fixed value for all the stack have been taken.

As it can be seen in Fig.3.2 and 3.3 there is a correspondence between Xb and X1. Xb is set manually in the lower image and X1 is the corresponding pixel value in the image obtained with high level of intensity

Once Xb and X1 have been calculated, the next step is to calculate Xa and its corresponding X2.

Xa is used to separate pixels that belong to the air with the rest of pixels that do not belong to the air. In order to calculate this threshold, three areas of air have been selected in every image obtained with high level of intensity. Xa is the average of the mean and the standard deviation in each area. It has been implemented by 3 function, white.m (where is selected the area that belong to the air), Xabove.m (where is calculated the mean and the standard deviation) and fused.m (the mean of the three where every image is charged).

Like in the previous case Xa is calculated from the high image and X2 is the corresponding pixel value in the image obtained with low level of intensity. X2 has been calculated with a similar algorithm as X1.

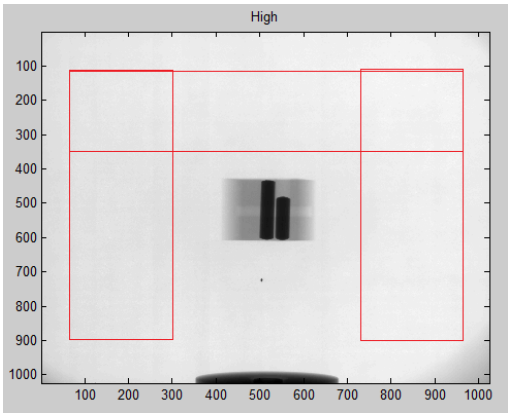

Figure II.4: Three areas belonging to the air in order to calculate Xa

When for every pair of images the thresholds have been defined it is time to create a new fused image:

When we have worked with “upscaling” and according with the section 3.1.1, for every pixel in the Low image if the value of gray level is smaller than Xb, in the fused image we have copied the corresponding (i,j) pixel from the High image, if on the other hand the pixel (i,j) in the Low image is bigger than X2 we have copied in the fused image the value of the pixel in the low image, for the rest of values in the low image between Xb and X2 we have applied the Eq3.3 corresponding with upscaling.

On the other hand, if we are working with downscaling, the process followed is similar; if the pixel (i,j) in the image taken with high level of intensity is smaller than X1, we have copied in the fused image this value. If the pixel in the High image has a value bigger than Xa, in the fused image we copied the corresponding pixel (i,j) that belong at the low image. For the rest of the pixels that there are between X1 and Xa we have applied the Eq3.6 corresponding with downscaling, section 3.1.2.

After this process we have all the new fused images in 3D matrix called $matrix_F$, and with the function writeback.m we have saved every image like file .float32, as it was in the beginning.

II.4 Performing of an experimental study

To develop this project, a little cube made of plastic (22x22x22mm) has been used as a model. The cube has three holes (Ø=4 mm) that pass through the cube, two transversally and the other longitudinally as it is showed in the next image.

Figure II.9: Photos of the cube

A cube with holes has been used in order to analyze firstly how the 3D reconstruction without metal is. Several features have been studied in the cube without metal so as to have a reference to compare afterwards the cube with the metal bars into it.

The numbers of projections obtained with the detector Metrotom have been three, with low, medium and high level of intensity. The detector Metrotom saves these stacks of 700 images consisting of several millions of pixels as a digital gray scale image to the image stack in files with the extension .float32. As these projections are stored with extension .float32 the gray levels are between 0 and 1.

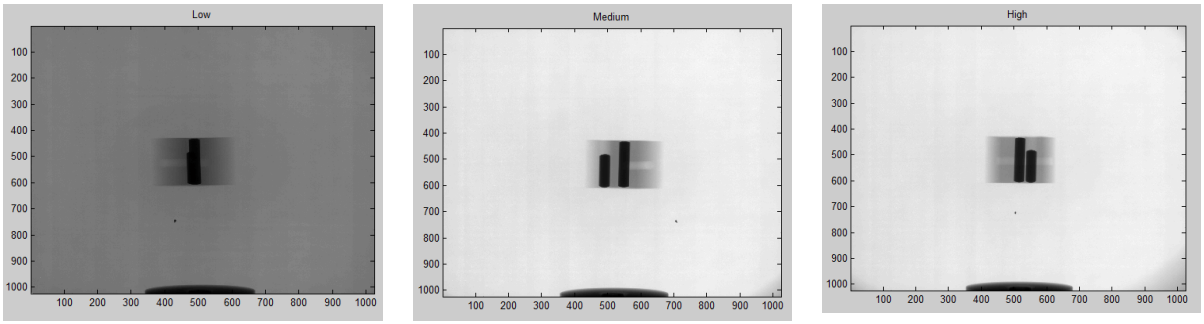

Figure II.10: Example of projections with different angles taken with low (left), medium (center) and high (right) level of intensity

As explained before, the work-piece has to be fixed to avoid movement during the acquisition of the image stacks. Thus, the corresponding pixels of a single projection represent the same area of the work-piece in the high and low-energy image. Due to this, pixels of different images can be compared and selected in order to create the new fused image.

The following table shows the parameters used for the CT- measurements.

	Tension(kV)	Current(μA)	Time of integration (ms)	Gain (pF)
High	220	370	800	1
Medium	150	370	800	1
Low	80	370	800	1

Table II.1: Parameters used for the CT-measurements

In the previous table can be seen that the maximum and minimum values of tension available in the Metrotom have been used.

The slices corresponding with the cube taken with high and low intensity have been reconstructed and analyzed. Hence the “maximum” values of artifacts have been obtained. Therefore the following measures will have like aim to reduce these artifacts.

The characteristics that have considered are the following:

- Mean and standard deviation both in the air and on the plastic
- Contrast between the different materials (air-plastic, plastic-metal), according to the definition made in ISO 15708-1:2002(E).
- Quantity and quality of the imaging artifacts (effect of beam hardening in cupping, streaks, dark bands, etc.)

Several reconstructions have been made:

VII. Reconstruction without metal bars inside.
VIII. Reconstruction with metal bars inside at high level of intensity
IX. Reconstruction with metal bars inside at low level of intensity
X. Reconstruction with metal bars inside through the fusion of the stack of images at high and low intensity with scaling (both upscaling and downscaling)
XI. Reconstruction with metal bars inside through the fusion of the stack of images at high and medium intensity with scaling (both upscaling and downsaling)
XII. Reconstruction with metal bars inside through the fusion of the stack of images at high and low intensity without scaling

The workflow used of the fusion process is shown below:

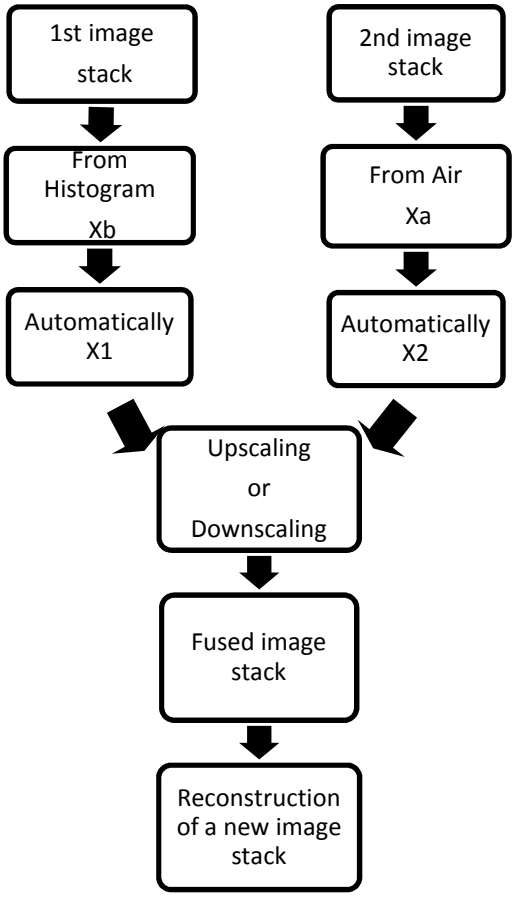

Figure II.11: Workflow of image stack fusion

Once a new stack of fused images is available a new 3D reconstruction has been made. Software called VG-Studio [VOLU10] has been used in order to analyze the results. About 300 slices in the plane XY are used to compare the different results. The plane XY has been chosen to make slices, because in this plane the two bars metal transversally with the artifacts produced is observed.

To quantify these results, a little software has been implemented too, in order to calculate the mean and standard deviation in a specific area and also another one to see the profile between the edges and the behavior of the pixels affected by artifacts, mainly the pixels that lie between the holes.

II.4.1 Experimental plan

The purpose of the experiments is trying to reduce the effect of the artifacts due to the two metal bars placed inside in the little cube made of plastic. For that, the stacks of images of the cube are three, each of them calculated with a different intensity, low, medium and high. Images taken with high intensity will be always present in the experiment, because as it has been mentioned earlier they are best suited for the reduction of artifacts. Hence fusions are going to be, low with high intensity, and secondly medium with high intensity. Fusions will be calculating using the scaling, with upscaling and downscaling, trying to obtain a characteristic

to make a difference between scales. Also there will be series of experiments without scaling to verify the importance of using a scale factor.

The idea that is going to be used in the experiments in order to find the correct below threshold, Xb, is looking for the most accurate value where finish the first peak in the histogram corresponding with the lower image. This value and the surrounding points will be used to find the best result to obtain a good contrast between the metal and the plastic, because the first peak corresponds with pixels that represent the metal.

The above threshold, Xa, will be calculated from the values of air, both with mean and standard deviation. The corresponding X1 and X2 are automatically calculated thanks to the software implemented. Once there are values for the four thresholds, Su or Sd is automatically calculated too.

It is important to be careful with this value, because for values of S lower zero than it is not possible to fuse the images with sense. A value of S lower than zero means that X1 is greater than X2 with the corresponding mixture with the pixels.

The first sets of experiments have been done by fusing the images taken with low and high level of intensity, because they are the two limits. The experiment will be considered satisfactory when some of the artifacts listed above (cupping, dark bands, streaks ...) are reduced without modifying other characteristics. Values of the reduction and the values of the threshold where the best result were obtained will have to be justified. To these sets of experiments will be applied both upscaling and downscaling.

The following tables show the positive results obtained, as positive are taken the experiments with values of Su bigger than zero.

	Xb	X1	X2	Xa	Su
Low-High	0,08	0,1886	0,2518	0,98	0,3681
Low-High	0,0818	0,192	0,2518	0,98	0,3516
Low-High	0,05	0,1224	0,2518	1	0,6411

Table II.2: Experiments with the stacks of images belong to Low and High level of intensity with upscaling

With the stacks of images from low and high level of intensity the thresholds Xb and Xa have been gradually spreading in order to have a positive value of the factor of scale Su. After to distance the threshold sufficiently, in principle an appropriate value for 3D reconstruction has been obtained, but without coinciding with the first idea of fusing.

After seeing the results with upscaling has been attempted to improve these results by using of downscaling, also is required a wide separation between thresholds for a positive value of Sd.

	Xb	X1	X2	Xa	Sd
Low-High	0,0818	0,192	0,2518	0,98	0,0798585
Low-High	0,05	0,1224	0,2518	1	0,1474

Table II.3: Experiments with the stacks of images belong to Low and High level of intensity with downscaling

Once the experiments fusing low and high images have been completed, the next sets of experiments will be with medium and high stacks of images, the objective of these measures will be to improve the results achieved previously. The way to achieve will be the same as applied before, to search the best value where finish the first peak in order to obtain the results with lower amount of artifacts.

Fusing by upscaling has been realized in first place. It has been adjusting the value where the first peak ends, obtaining improvements with the successive reductions, while the value of the scale factor, Su, increases. These experiments and values of the different thresholds are shown in the next table.

	Xb	X1	X2	Xa	Su
Medium-High I	0,2	0,3191	0,5776	0,9	0,6846
Medium-High II	0,1809	0,286	0,5668	0,8845…	0,7277
Medium-High III	0,1601	0,2497	0,5668	0,8845…	0,7798

Table II.4: Experiments with the stacks of images belong to Medium and High level of intensity with upscaling

The suspension points in the square of the threshold Xa indicate that there is a new value calculated from the air for each pair of medium-high images.

Finally, fusions have also been made with stacks of images of medium and high intensity using the method of downscaling.

	Xb	X1	X2	Xa	Sd
Medium-High I	0,2	0,3191	0,5668	0,8845…	0,4381
Medium-High II	0,1671	0,2626	0,5668	0,8845...	0,4892

Table II.5:Experiments with the stacks of images belong to Medium and High level of intensity with downscaling

Experiments will be also carried out by fusing images without the use of scaling, to verify that a scaling of one image stack to fit the other has to be done using a scaling factor, because two image stacks have been acquired using different energies and thereby the corresponding pixels of two projections do not have matching gray values.

II.4.2 Ground truth and criteria for evaluation

As presented in the chapter 1.3 Structure of the work, before to start to fuse stack of images, a reference is needed and therefore the cube without metal has been analyzed.

In order to make a difference with projections, and to avoid doubts, all the slices obtained from VG-Studio are stored as files with extension .raw, for this reason the levels of gray here are between 0 and 65535.

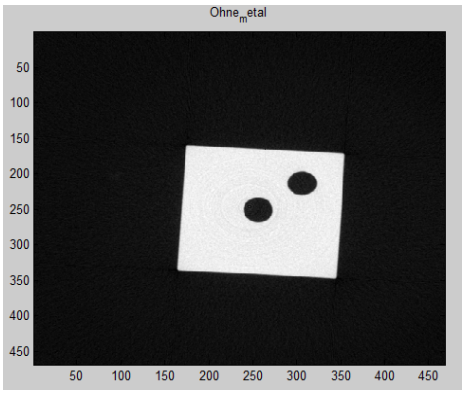

Figure II.12: Slice from the cube made of plastic without metal bars inside

As it is shown in the Fig.4.4, the slice from the cube made of plastic without metal bars does not present almost any artifact and all the edges are sharp both inner and outer. After analyze different central slices in different positions as a result, there are between 4-5 pixels and 30000 levels of gray between the air and the plastic.

Moreover the average value of the pixels both in the air and in the plastic has been calculated, to this end several areas that belongs to the air and the plastic have been selected giving as a result in the plastic a value of 44500 gray levels with a standard deviation near to 85. In the area of the slice that belong to the air the value of the mean and standard deviation have been calculated too, the results have been 11700 gray level with a deviation of 50.

In addition, the cube with metal bars inside taken with a high level of intensity also has been analyzed. As it has been explained before, images taken with high levels of intensity reduce the potential for the appearance of artifacts, so these values are the limit which are going to try to be overcome.

The artifacts are visible in the Fig.4.5 after doing the 3D reconstruction, it can clearly be distinguished the cupping, the streaks and dark bands in the vicinity of the metal bars.

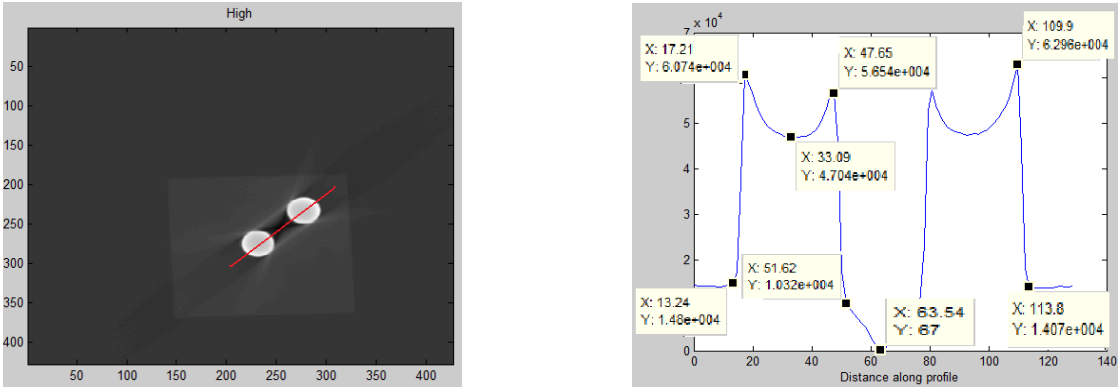

Figure II.13: Slice from the cube with metal bars inside taken with a high level of intensity and the corresponding profile along the holes

In an area not affected by artifacts between the air and the plastic there are 5-6 pixels and about 2250 gray levels in the edges. However the change in the edges where the metal bars are, it is quite different.

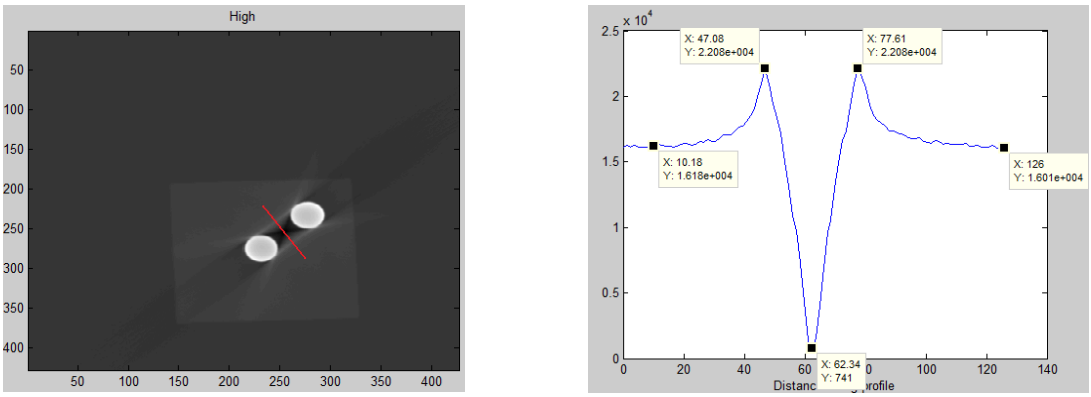

Figure II.14: Slice from the cube with metal bars inside taken with a high level of intensity and the corresponding profile across the holes

Between the plastic and the metal there are only about 4-5 pixels similar with the previous cases, not as the gray level jumps, which is about 47000.

The effect of the cupping is more visible here and due to its cupping-shaped, because of its name. Although all the circle is the same material, metal, with theoretically the same value of gray level, there are a big different between the border and the middle, exactly 13700 levels of gray, there is a reduction of 21.67% between the maximum value, 60000, and the lower at the bottom of the cup, this variation is an important value that will be tried to be reduced.

The value of the mean and the standard deviation free of artifacts in the plastic is 16000 and 100 respectively. Amongst the holes, there is an area which is plastic and supposedly it should be with the same value of gray level, but due to the beam-hardening effects there are dark areas that made this not possible. As it can be seen in the corresponding profile, there are important variations with respect at the mean value in the plastic, with pixels 37.5% above average and others almost with a value of 0.

The mean in the air is 13600 with a standard deviation of 25, as it can be seen, working with a high level of intensity there are just a difference of 2400 gray levels between the mean in the plastics and the air.

The stack of images taken with low level of intensity has also been analyzed as reference.

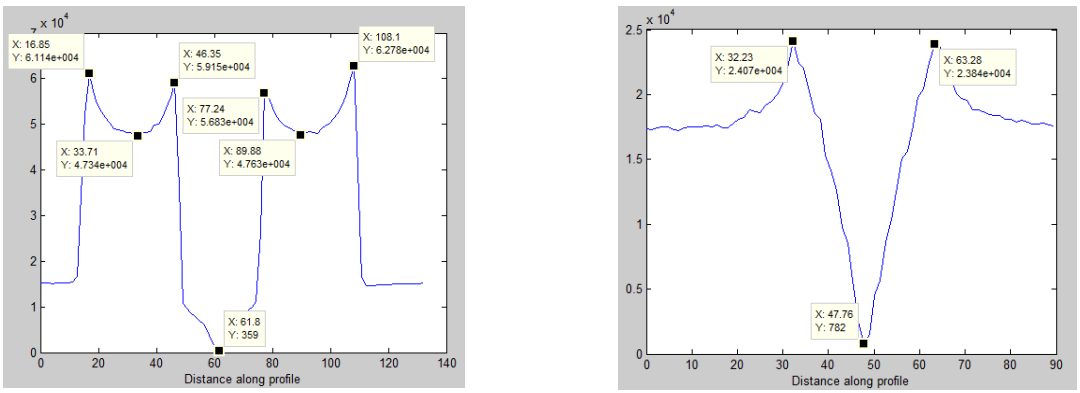

Figure II.15: Profiles from the cube with metal bars inside taken at low intensity, along (left) and across (right) the holes

In the stacks of images taken with low level of intensity the average in the air free of artifacts is 15400 gray levels and 17200 in the plastic, it is means, a difference of 10.47%.

The values both cupping and dark bands are very similar with the case of images taken with high intensity, there are difference of 24.08% in the cupping and in the dark bands points 39.50% bigger and another 95% smaller.

II.4.3 Presentation of the result with fusion

After several tests fusing stack of images, applying the two options of scaling, which have been presented in the section 3.1 Theoretical Basic, here are explained and commented the more important results.

The results are shown according to the point 4.1 Experimental Plan.

II.4.3.1 Fusion with Low-High energy images stacks

The method applied was as follow, in the Fig.4.8 are shown the histogram corresponding with the first image taken with low intensity (left) and the first one taken with high intensity (right), as it was explained in the section 3.2 Implementation of the algorithm by using Matlab. From the histogram of the image of low intensity have been selected manually the first threshold Xb, where finish the first peak. Thus, the values darker from the less dark can be separated, in other words, the pixels corresponding with metal are separated.

It would be good to clarify, that the colors displayed on the slices do not correspond with the black (0) and white (1) represented in the histogram. In histograms the first peak (left) corresponding with the metal (which more X-ray absorbed) but in the slice is white, the second with the plastic and the third and bigger with the air, in accordance with the histogram the air would be white and the metal black but Matlab paint this upside down. It is important to have this clear to avoid errors of interpretation.

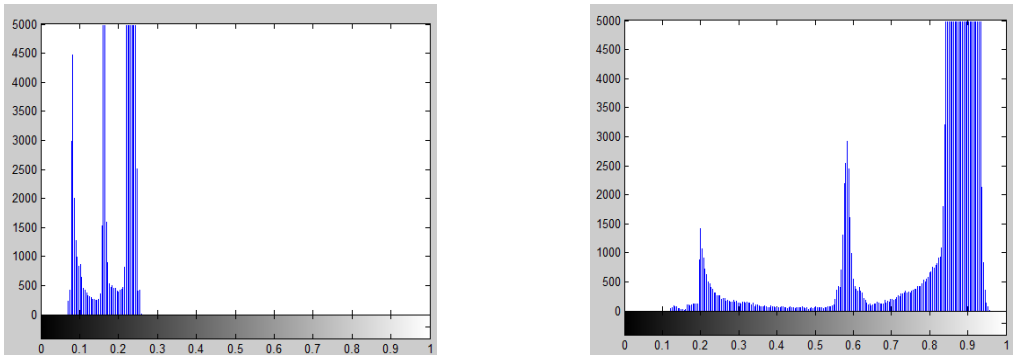

Figure II.16: Histograms of the first image taken with low intensity (left) and the first with high intensity (right)

In view of the big differences between the two histograms and taking into account the method to fuse images, the hopes to get something representative were not very high, because as it can be seen in the Fig. 4.9 the curves corresponding to the low and high intensity are far apart, thus to avoid an overlap between X1 and X2 the threshold Xb and Xa should be widely separated.

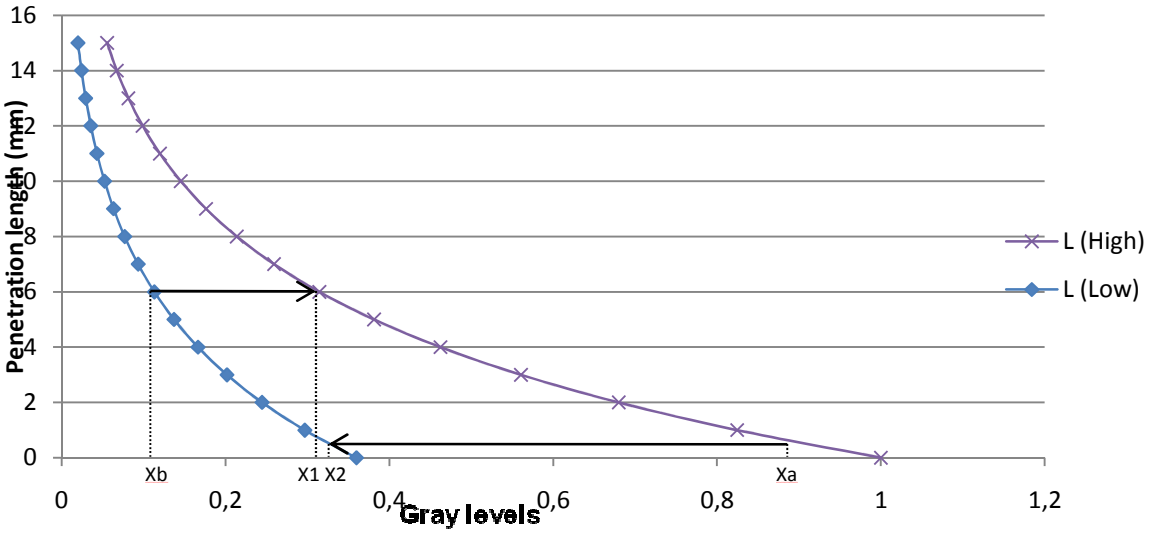

Figure II.17: Logarithmic function between the low and the high stacks of images

We started taken from the histogram a value for Xb where the first peak finish, it is mean Xb=0.1371, and Xa was directly 0.9, regardless of the value from the air because the values should be widely separated. Once Xb and Xa have been selected the corresponding X1 and X2 are automatically calculated, the factor of scaling S (Su in this case because it is upscaling) is calculated too.

As expected Su was smaller than zero, after many test to avoid X2 is less than X1, we were able to fuse the images with an value of Xb=0.0818 and Xa=0.98, thereby taking a value of Su=0.3516, but this value do not meet our original intention, because Xb is smaller than the final value of the peak, and Xa is much greater than the value of the mean air. Anyway the reconstruction and subsequent analysis have been continued.

Although Su is bigger than 0, the conditions for the calculation of thresholds have not been carried out, for this reason the results obtained were not good, as is shown in the Fig.4.10.

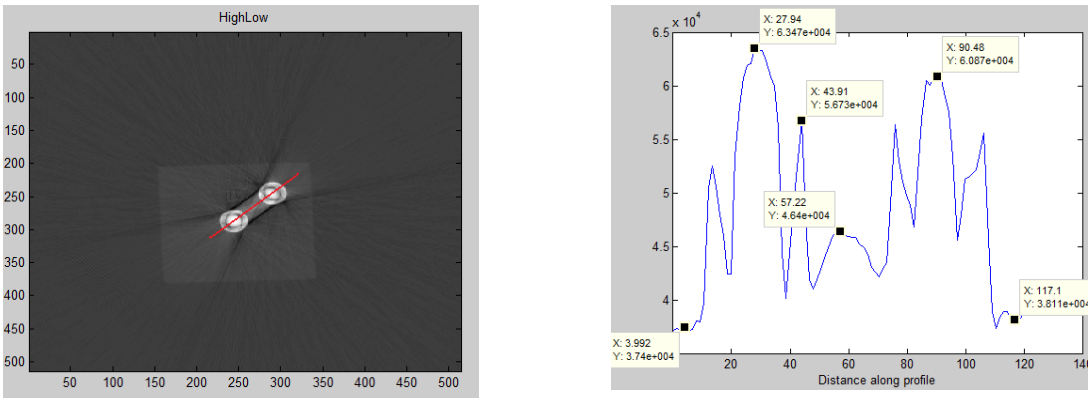

Figure II.18: Fusion with images from Low and High intensity, slice (left) and profile (right)

At first glance, in the slice can be seen the large number of artifacts present, which are then quantified in the profile, profile corresponding to the line that passes through the two circles.

The fusion of images from low and high intensity is discarded for both upscaling and downscaling, in upscaling the results from the 3D reconstruction are clear, and with the

downscaling because in order to have a value of Sd bigger than zero you need a value of Xb smaller 0.08 and Xa bigger than 0.95, this means do not carried out with the proposed conditions, obtained similar results to the upscaling. For this reason it is not necessary to make the 3D reconstruction.

II.4.3.2 Fusion with Medium-High energy images stacks

Ruled out the fusion between images of low and high intensity using this method, experiments have been based on image fusion of medium and high intensity. It has been proceeded as in the previous case. Starting working with upscaling, and then compare these values with those obtained by downscaling.

As it can be seen in Fig.4.11, the curves corresponding with medium and high intensity are closer than in the case of low and high intensity, for this reason have been easier to fuse the corresponding stacks of images, obtaining a correct value of Su.

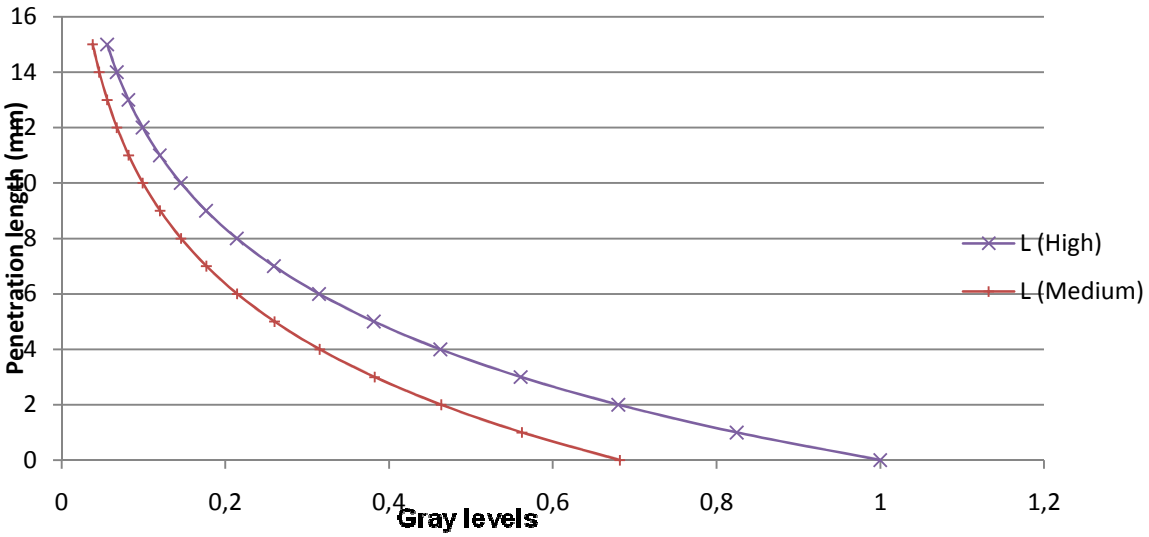

Figure II.19: Logarithmic plot that display images taken with medium and high intensity

This closeness can be also observed in the following histograms, on which the calculation of threshold has been based.

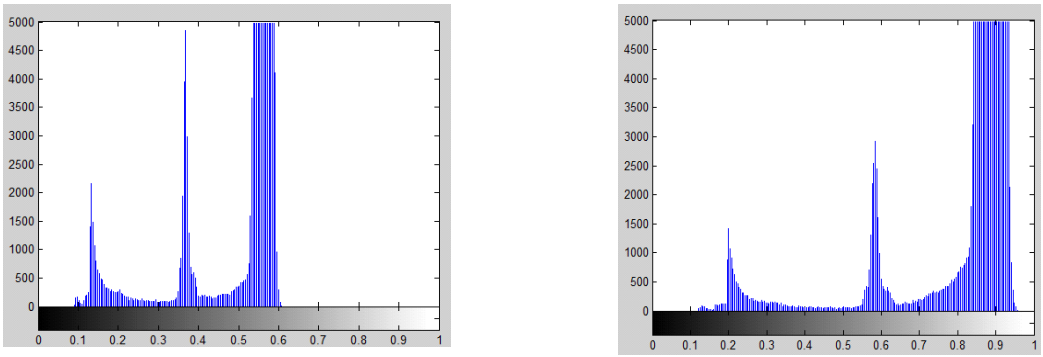

Figure II.20: Histograms of the first image taken with medium intensity (left) and the first with high intensity (right)

The selection of the below threshold, Xb, have to be careful, because a small change in the value of this threshold changes significantly the scaling factor. The first results shown here

are with Xb=0.2 and Xa=0.9, obtaining in this case the value of Su=0.6846. There is no problem with the overlap between X1 and X2.

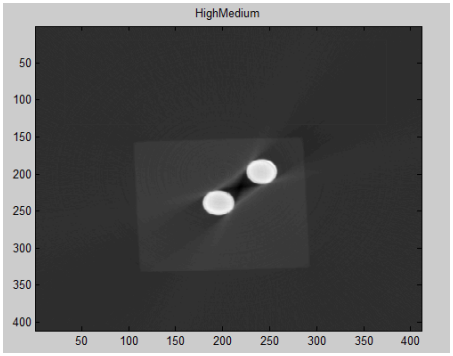

Figure II.21: Slice from the fusion of images taken with medium and high intensity

At first glance, Fig.4.9, the improvements are evident with respect to the fusion of low and high intensity, obtaining a slice more similar to that obtained only with high intensity.

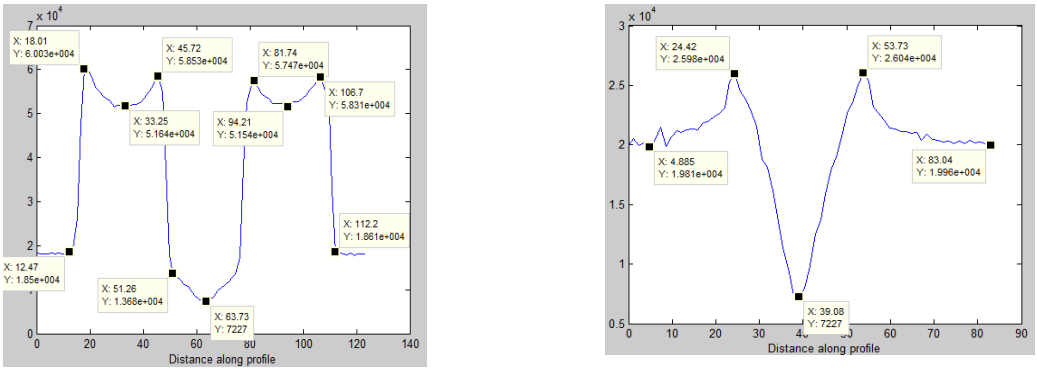

Figure II.22: Profile of the metal bars and plastic, along (left) and across the circles (right). Upscaling fusion I

The fusion of the stack of images taken with medium and high intensity have allowed us to see the first improvements due to the reduction of the artifact called cupping and reducing the effect of the black bands.

On the one hand, as it can be seen in the Fig.4.10 the values of cupping has been reduced, obtaining a difference near to 8400 gray levels, smaller than 13700 that there was without fusion, the reduction of 21,67% now it is just of 14%.

On the other hand, when the profile across the circles has been analyzed, it can be seen that the minimum value between the holes has been increase, now it is near to 7000 where before it was almost zero. Thus, the difference now is not so big, 63.82% instead of 95.38% previous. In this case the mean in the plastic is 19900, and there are values 30.65% bigger, better than 37.50% that there was in the high slice. In the air the value of the mean is 17500 gray levels.

With regard to the contrast there are no significant differences, because the change between the air and plastic are still 5-6 pixels.

Once obtained this improvement, the next step was to reduce more these artifact. Others 3D reconstructions have been carried out with a few changes until obtained these

improvements. Now the threshold Xb has been more exacted. The Xb value has been fixed to 0.1809 and the above threshold has been left free to be automatically calculated for each image from the three areas belonging to the air, where for example the first Xb is 0.8845. These values of threshold give a factor of scaling Sd equal to 0.4381.

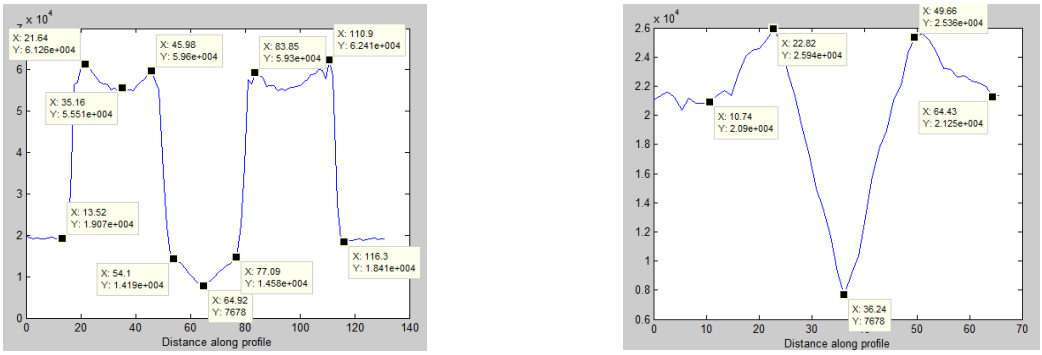

Figure II.23: Profile of the metal bars and plastic, along (left) and across the circles (right). Upscaling fusion II

There have been some improvements, reducing the cupping effect until a value near to 6500, 9% of deviation, and the effect of the dark bands or streaks too. Now there are only values 25.60% bigger and 63.29% smaller, because the average has increased slightly and has decreased the maximum value.

For the next experiment has been chosen a value of Xb equal to 0.1601, as it can be seen in the Fig.4.12, this point is not where finish the peak, if not it is within the peak. This experiment has been made to see if the artifacts are more reduced or on the contrary compromising the other features, like in the case of fusion with low-high intensity.

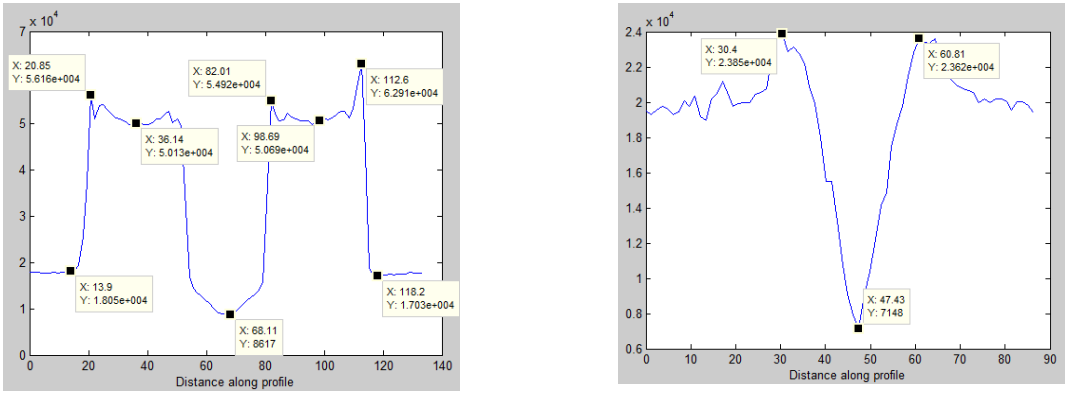

Figure II.24: Profile of the metal bars and plastic, along (left) and across the circles (right). Upscaling fusion III

As it is plotted in the Fig. 4.16, if the value of the threshold is not where the peak ends, the results begin to be incongruous, because we have lost values corresponding with the metal when we have chosen the threshold. In the cupping-shaped there are high values, which make increased the difference between the high value and the bottom of the cup in 18.39%. With regards to the dark bands there is a little improvement, but very similar with the previous experiment.

Once the fusion of images stack using upscaling has been analyzed, it is time to check if there are improvements or drawbacks with the downscaling.

By using upscaling it can be seen that with a new value for the threshold Xa for every pair of images the artifacts are smaller, thus, with in this way we have worked. Besides the value to Xb has been 0.2 to start with the experiments as in upscaling.

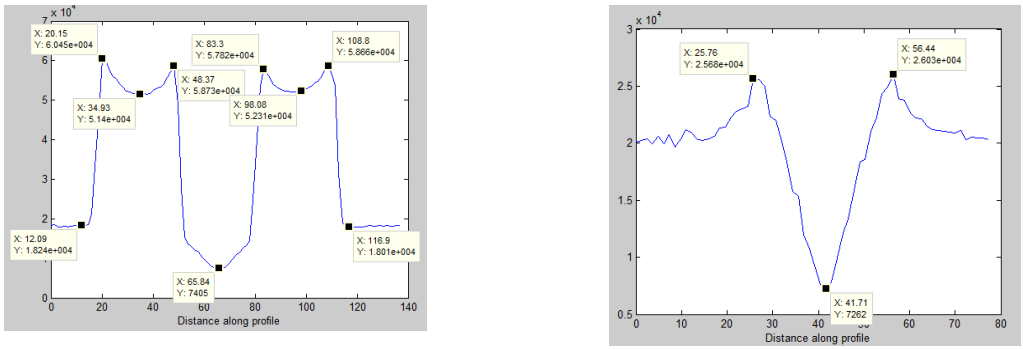

Figure II.25: Profile of the metal bars and plastic, along (left) and across the circles (right). Downscaling fusion I

The average value in the air is 17600 and 19850 in plastic. On the one hand, in metal the highest value is 60500 and the lower 51400, which means 15.04% of cupping, and on the other hand the highest value in the plastic across the holes due to the dark bands is 26000 and the lower 7200. Therefore there are values 31% bigger and 63.73% smaller.

Despite being a proper result, the first test with downscaling is not as suitable as the one obtained with upscaling. The following experiments will aim at reducing artifacts. To this end, a value closer to the peak center have been chosen, Xb=0.1671, but a little closer to the end of the peak, because with the value of 0.1601 problems in upscaling have been observed.

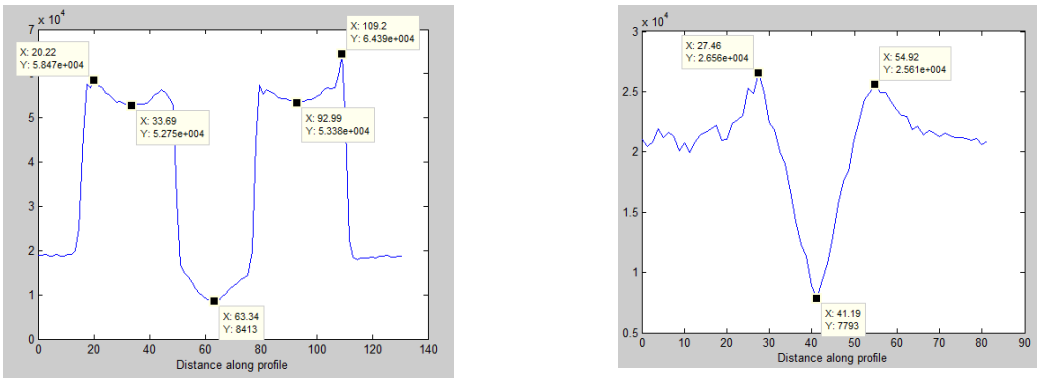

Figure II.26: Profile of the metal bars and plastic, along (left) and across the circles (right). Downscaling fusion II

The values are not very good, due to the value of Xb chosen has not been the correct, because it has been further to the end of the peak as it has been expected to. As a result there have been downturns both in the difference between in air and plastic and in the effect of beam hardering over cupping.

In any case the average in the air has been 17875, and 20550 in the plastic, which means a difference of 13%. In regards to cupping, the maximum value in the metal is 64400 and the minimum 53300, resulting 17.24% of difference.

On the other hand the values due to dark bands are similar than in the previous case, with maximum values of 23850 and minimum of 7100.

II.4.3.3 Fusion without scaling

After fusing the stacks of images using the scaling, a new experiment was carried out to check how the results without the use of scaling would be. The idea is to take the group of pixels from one image or another in order to try to obtain a proper contrast between the different materials. As it has been shown in the previous experiments, differences between air and plastic are not too big.

The pixels belonging to one of this “materials” (metal, plastic and air) in every of these following plots, make a group around values of gray level. The first peak in every plot correspond with the metal (the darkest, values), the second with the plastic and the last peak with the air.

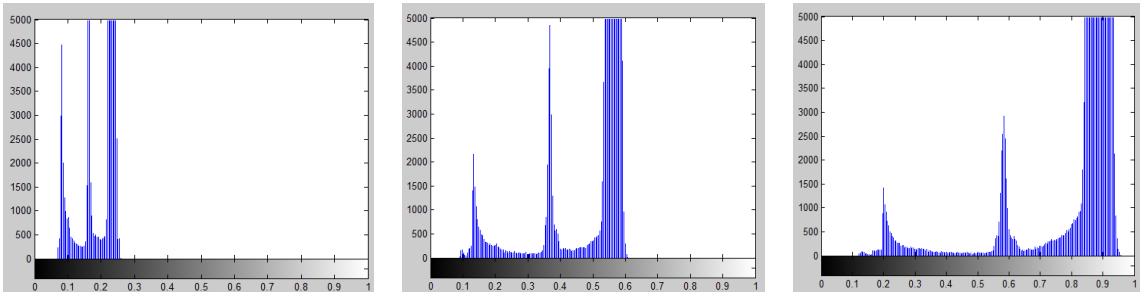

Figure II.27: Low (left), medium (center) and high (right) histogram

Firstly, the low and the high image are going to be fused. From the image taken with low intensity, the pixels selected are the one below 0.1, belonging to the metal and above 0.2 belonging to the air. Consequently, the pixels between 0.1 and 0.2, which belong to the plastic are taken from the image of high level of intensity.

So as to clarify this explication, a part of the program is attached:

With low intensity

If matrixL(i,j,h) <= 0,1 or if matrixL(i,j,h) >= 0,2

matrixF(i,j,h)=matrixL(i,j,h)

else

matrixF(i,j,h)=matrixH(i,j,h).

Therefore, the corresponding 3D-reconstruction has been obtained, although the results without scaling are not good.

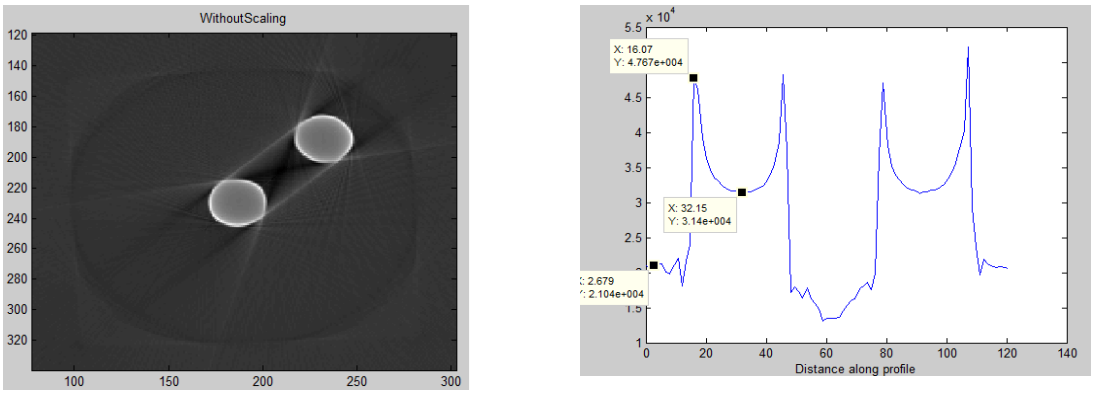

Figure II.28: Slice from low and high images without scaling and profile of the metal bars and plastic along the circles.

The aim of this experiment is to obtain a better contrast and difference between the air and the plastic but the results have worsened. The first problem is that there is no more a square,but something similar to an egg. The values in outer edges do not have a specific measure. In addition, the value of the cupping has been increased. In conclusion,it does not make sense working without scaling.

II.5 Evaluation of the results

Once all the experiments have been carried out and presented, it is time to evaluate the results. The goal of all these experiments were to reduce the amount of artifacts produced mainly by beam hardening presented in the slices, quantifying these artifacts and comparing with the initial values without any kind of fusion.

The more visible artifacts in the slices are cupping and dark bands so our experiments have been based on them. On the next page, the Table 5.1 shows a summary of all the important results, which are going to be commented in the following paragraph.

Firstly, a significant reduction of the artifact known as cupping has been obtained. Initially, the maximum value in the metal was near to 60000 gray levels and due to the beam-hardening the smaller value was 47000, which means that there was a reduction of 21.67%. After fusing the medium stack with the high stack through the upscaling it was possible to reduce this value to 9.02%, maintaining approximately the same maximum value in the metal.

Secondly, there have also been some improvements with regards to dark bands present between the holes. At the beginning, working only with the 3D reconstruction according to the stack of high images, without fusion, the average value in the plastic free of artifact was 16000, the maximum value owing to the beam-hardening was 22000, and the minimum 700, therefore there were values over 37.50%, and below 95%. After the fusion using upscaling the mean value of plastic has risen to 20700 and the maximum value due to the black bands have risen at 26000 and the minimum to 7600. Finally, there have been values over 25.60% and below 63%. This fact holds a decrease of the previous values, from 37.50% to 25.60%, without any kind of fusion.

Working with upscaling and downscaling, we were not able to increase the contrast between air and plastic. Moreover this contrast has been reduced. When the cube without metal was analyzed, there was observe a contrast of almost 33000 gray levels between air and plastic, since 17500 in the air until 44500 in the plastic, a 73.7% of variation. Afterwards, when the reconstruction of the stacks of images taken with high level of intensity has been made, the difference was only 2500 levels of gray, from 13600 in the air until 16000 in the plastic, which means, only a 15% of variation, far away from the values without metal.

This variation of 15% has not been able to be increased with the different experiments. This value has been always lower using both the upscaling and downscaling.

To sum up, with this method of scaling the fusion of two different stacks of images is not possible where its corresponding logarithmic curves are far apart, (see 4.3.1 Fusion with Low-High energy images stacks). Due to the thresholds, Xb and Xa, must be widely separated so as to avoid the cross between X1 and X2 and the subsequent mixture of pixels. When Xb and Xa are separated more than necessary the initial conditions are not met and the results do not show improvements.

On the one hand, it is observed that the scaling is necessary in order to obtain a good contrast between different materials. Without this scale the edges are not sharp and the results, as it can be seen in the Fig. 4.16, are not good at all.

On the other hand, the reduction of cupping and dark bands is possible with an accuracy selection of the below threshold. As it can be seen in the fusion Medium-High III with upscaling, and Medium-High II with downscaling, the choice of an incorrect value for Xb, choosing below the end of the first peak, produces an increase or artifacts and a loss of pixels corresponding to the metal.

					Cupping			Dark bands			
	Air´s r	Plastic´	Nº of pixels betv		Max	Min	Cupping	Max	Min	points..bigger	points..smaller
Cube without metal	11700	44500	5-6	73,71%	0	0	0	0	0	0%	0%
Cube at high level of intensity	13600	16000	5-6	15,00%	60000	47000	21,67%	22000	740	37,50%	95,38%
Cube at low level of intensity	15400	17200	5-6	10,47%	62700	47600	24,08%	24000	780	39,53%	95,47%
Upscaling											
High-Medium I Xb=0,2	17500	19900	5-6	12,06%	60000	51600	14,00%	26000	7200	30,65%	63,82%
High-Medium II Xb=0,1809	18050	20700	5-6	12,80%	61000	55500	9,02%	26000	7600	25,60%	63,29%
High-Medium III Xb=0,1601	16650	19350	5-6	13,95%	62000	50600	18,39%	23850	7100	23,26%	63,31%
Downscaling											
High-medium I Xb=0,2	17600	19850	5-6	11,34%	60500	51400	15,04%	26000	7200	30,98%	63,73%
High-medium II Xb=0,1671	17875	20550	5-6	13,02%	64400	53300	17,24%	26000	7800	26,52%	62,04%

Table II.6: Overview importants results

II.6 Conclusion and Outlook

The inspection of industrial work pieces using computed tomography has great potential in the field of material testing and non-destructive testing. In this Master Thesis, a method for dealing with work-pieces of high aspect ratios and differently absorbing materials in measurements using computed tomography has been shown.

The results obtained are positives, as the artifacts have been reduced, but not completely. As it can be observed within the different results, both cupping and the effect of dark bands have been decreased without affecting the other characteristics too much. It is also true that the contrast between air and plastic has been reduced, only 3%, but it is negative anyway.

The fusion of stacks of images taken at different intensities is a method still in development. It is true that further reduction of artifacts and better differentiation between the different materials were expected.

For future researches is recommended the correction of the beam hardening (see [TUY83], [MORI81], [DEMA00], [KRUM08], [BARR04], [HSIE98]) prior the fusion of the stacks of images to prevent this high occurrence of artifacts, because only with the fusion it is not possible to eliminate beam hardening and it would be advisable a previous weakening.

In future researches, it would be good to find a way to take up the entire width of gray levels, in order to have a proper separation between the different materials, because this part has been the only one, in which we have not been successful. On the other hand, the stack of images from which we started was not much better.

III Tabla de símbolos y abreviaciones

TC	Tomografía Computerizada
FBP	Filtered back projection (retroproyección filtrada)
HDRi	High Dynamic Range Imaging (imágenes dinámicas de alto rango)
h	Constante de Plack
c	Velocidad de la luz
λ	Longitud de onda
I	Intensidad remanente
Io	Intensidad inicial
L	Grosor del material
μ	Coeficiente de atenuación lineal del material
Xb	Umbral inferior
X1	Umbral correspondiente con el umbral inferior
Xa	Umbral superior
X2	Umbral correspondiente con el umbral superior
Su	Factor de escalado superior
Sd	Factor de escalado inferior

IV Índice de figuras y tablas

V Bibliografía

[HEIN08] Heinzl, C.; Analysis and Visualization of Industrial CT Data, Altschwendt, Dezember 2008

[HSIE03] Hsieh, J.: Computed tomography: Principles, design, artifacts, and recent advances. Ed SPIE, The Society of Photo-Optical Instrumentation Engineers 2003

[KRÄM10] Krämer, P.; Wechenmann, A.; Multi-energy image stack fusion in computed tomography. Chair Quality Management and Manufacturing Metrology, University Erlangen-Nuremberg, Germany, February 2010

[ZEIM10] Products Metrotomography, Metrotom 1500, http://www.zeiss.com/metrotom

[WECH09] Wechenmann, A.; Krämer, P.; Application of computed tomography in Manufacturing Metrology, Print ISSN: 0171-8096, Volume: 76, 07/2009, p. 340-346

[CSEP10] http://csep10.phys.utk.edu/astr162/lect/light/spectrum.html

[MAHN03] Mahnken, A,; A New Algorithm for Metal Artifact Reduction in Computed Tomography; Department of Diagnostic Radiology, Aachen University of Technology

[KRUM08] Krumm, M.; Kasperl, S.; Franz, M.; Referenceless Beam Hardening Correction in 3D Computed Tomography Images of Multi-Material Objects. 17th World Conference On Nondestructive Testing, Oct 2008, Shanghai, China.

[BARR04] Barrett, Julia F.; Keat, N.; Artifacts in CT: Recognition and Avoidance; Radiographics 2004 Nov 24(6) 1679-91.

[HSIE98] Hsieh, J.; Adaptive streak artifact reduction in computed tomography resulting from excessive X-ray photon noise. Applied Science Laboratory, GE Medical System, Milwaukee, Wisconsin 53201. 1998.

[DEMA00] De Man, B.; Nuyts, J.; Dupont, P.; Marchal, P.; Suetens, P.; Reduction of metal streak artifacts in X-ray computed tomography using a transmission maximum a posteriori algorithm. IEEE Transactions on Nuclear Science, vol. 47, nr. 3, 2000, P. 977-981.

[MORI81] Morin, R.; Raeside, D.; A Pattern Recognition Method for the Removal of Streaking Artifact in Computed Tomography, October 1981.

[TUY83] Tuy, H.K.; A post processing algorithm to reduce metallic clip artifacts in CT images. Eur Radiol. 1993; 3; P. 129-134.

[WANG96] Wang, G; Snyder, D. L.; O´Sullivan, A.; Vannier, M.W.; Iterative deblurring for CT metal artifacts reduction. IEEE Trans Med Imaging. 1996; 1: 657-664

[WECK09] Wechenmann, A.; Krämer, P.; Application of Computed Tomography in Manufacturing Metrology; Friedrich-Alexander-Universität Erlangen-Nürnberg 2009

[KAST04] Kastner, J.; Schlotthauer, E.; Burgholzer, P.; Stifter, D.; Comparison of X-ray computed tomography and optical coherence tomography for characterisation of glass-fibre polymer matrix composites, In Proceedings of World Conference on Non Destructive Testing (2004), pp. 71-79

[FELD84] Feldkamp, L.A.; David, L.C.; Kress, J.W.; Practical cone-beam algorithm. Journal of the Optical Society of America A 1(6), 612-619.1984

[GOSH05] Goshtaby, A. ; 2-D And 3D Image Registration For Medical, Remote Sensing, And Industrial Applications, John Wiley & Sons Inc, 2005

[DERE94] Derek, L.G.; Accurate Frameless Registration of MR and CT Images of the Head: Applications in Surgery a Radiotherapy Planning; Dept. of Neurology, United Medical and Dental Schools of Guy,s and St. Thomas´s Hospitals, London, Set 9R, U.K., 1994

[BLUM05] Blum, R.S.; Liu, Z.; Multi-sensor image fusion and its applications (special series on Signal Processing and Communications), Taylor & Francis, CRC Press; July 2005

[MYSZ05] Myszkowski, K.; High Dynamic Range Techniques in Graphics: from Acquisition to Display; Eurographics 2005 Tutorial T7

[VOLU10] VGStudio Max http://www.volumegraphics.com/products/vgstudiomax/